

Article

Green Synthesis of Gold Nanoparticles Using Liquiritin and Other Phenolics from *Glycyrrhiza glabra* and Their Anti-Inflammatory Activity

Ali O. E. Eltahir¹, Kim L. Lategan² , Oladipupo M. David² , Edmund J. Pool², Robert C. Luckay³ 
and Ahmed A. Hussein^{1,*} 

¹ Chemistry Department, Cape Peninsula University of Technology, Bellville 7535, South Africa; aliomers250@gmail.com

² Department of Medical Bioscience, University of Western the Cape, Bellville 7535, South Africa; klategan@uwc.ac.za (K.L.L.); 3681075@myuwc.ac.za (O.M.D.); epool@uwc.ac.za (E.J.P.)

³ Department of Chemistry and Polymer Science, Stellenbosch University, Matieland, Stellenbosch 7602, South Africa; rcluckay@sun.ac.za

* Correspondence: mohammedam@cput.ac.za

Abstract: Phenolic compounds are the main phytochemical constituents of many higher plants. They play an important role in synthesizing metal nanoparticles using green technology due to their ability to reduce metal salts and stabilize them through physical interaction/conjugation to the metal surface. Six pure phenolic compounds were isolated from licorice (*Glycyrrhiza glabra*) and employed in synthesizing gold nanoparticles (AuNPs). The isolated compounds were identified as liquiritin (1), isoliquiritin (2), neoisoliquiritin (3), isoliquiritin apioside (4), liquiritin apioside (5), and glabridin (6). The synthesized AuNPs were characterized using UV, zeta sizer, HRTEM, and IR and tested for their stability in different biological media. The phenolic isolates and their corresponding synthesized NP conjugates were tested for their potential in vitro cytotoxicity. The anti-inflammatory effects were investigated in both normal and inflammation-induced settings, where inflammatory biomarkers were stimulated using lipopolysaccharides (LPSs) in the RAW 264.7 macrophage cell line. LPS, functioning as a mitogen, promotes cell growth by reducing apoptosis, potentially contributing to observed outcomes. Results indicated that all six pure phenolic isolates inhibited cell proliferation. The AuNP conjugates of all the phenolic isolates, except liquiritin apioside (5), inhibited cell viability. LPS initiates inflammatory markers by binding to cell receptors and setting off a cascade of events leading to inflammation. All the pure phenolic isolates, except isoliquiritin, neoisoliquiritin, and isoliquiritin apioside inhibited the inflammatory activity of RAW cells in vitro.

Keywords: *Glycyrrhiza glabra*; licorice; liquiritin; phenolic compounds; gold nanoparticles; lipopolysaccharide; cell viability; anti-inflammatory



Citation: Eltahir, A.O.E.; Lategan, K.L.; David, O.M.; Pool, E.J.; Luckay, R.C.; Hussein, A.A. Green Synthesis of Gold Nanoparticles Using Liquiritin and Other Phenolics from *Glycyrrhiza glabra* and Their Anti-Inflammatory Activity. *J. Funct. Biomater.* **2024**, *15*, 95. <https://doi.org/10.3390/jfb15040095>

Academic Editor: John H.T. Luong

Received: 28 February 2024

Revised: 29 March 2024

Accepted: 2 April 2024

Published: 6 April 2024



Copyright: © 2024 by the authors. Licensee MDPI, Basel, Switzerland. This article is an open access article distributed under the terms and conditions of the Creative Commons Attribution (CC BY) license (<https://creativecommons.org/licenses/by/4.0/>).

1. Introduction

Various chemical and physical syntheses of nanoparticles have been applied for the biosynthesis of AuNPs [1,2]. Physicochemical properties can have substantial effects, such as target-binding activities, and increase tolerance toward biocompatibility [3]. The combination of a high specific surface area, safety, biocompatibility, and the ability to easily modify their surfaces, along with gold's strong affinity for sulfur atoms and its remarkable cell and tissue penetration capabilities, position AuNPs as a superb platform for diagnostics and therapeutics in the field of biomedicine. Furthermore, incorporating well-defined capping agents with a safety margin and established pharmacological profiles has the potential to expand the significance of AuNP/natural product conjugates, creating a novel and valuable platform for addressing inflammation [4–8].

A fundamental understanding of the nanoparticle's surface and the capping agents' nature is crucial for designing and developing well-characterized nanomaterials [9].

Green synthesis, in line with green chemistry principles, provides many advantages. One of these benefits is the utilization of abundant, easily accessible, and affordable biodegradable natural sources that serve as efficient reducing and stabilizing agents. Furthermore, eco-friendly solvents are frequently employed, safeguarding the environment against detrimental chemical residues. Moreover, the nanoparticles produced through green synthesis demonstrate considerably reduced toxicity levels [10,11].

Particular interest has been directed towards using natural products as reducing and capping agents [12], and AuNPs capped with different phenolic compounds such as epigallocatechin gallate (EGCG) [13], mangiferin [14], quercetin [15], proanthocyanidin dimer [16], hypoxoside [17,18], hesperidin [19,20], and tricetin have been reported [21]. Capping agents, in most cases, are responsible not only for the stability of the NPs but also for enhancing their activity and selectivity [22,23]. Due to the chemical nature of the phenolic compounds, they can form, stabilize, and activate the AuNPs. Phenolic compounds are widely distributed in nature and have essential biological functions in plants [24,25]. Additionally, they have a wide range of pharmacological properties and are beneficial for human health [25–27].

Licorice (*Glycyrrhiza glabra*) is a known medicinal plant that has a wide range of traditional and pharmacological activities. The chemistry of the plant has been studied extensively and several types of flavonoids and triterpenoid glycosides have been shown [28]. Different biological activities, including the anti-inflammatory activity of the total extract and some isolated compounds, have been reported in vivo and in vitro [29,30].

The future application of metal NPs as biological modulators in treating various human pathologies depends on the presence of both safe and bioactive conjugates with well-defined structures. Fulfilling these requirements entails employing green technology for safety purposes and utilizing active capping agents that are singular and well-defined, moving away from the use of total extracts. Continuing our research endeavors, we strive to employ well-defined metal NP conjugates with medicinal applications [17,18,31]. This study presents the green synthesis and characterization of six newly synthesized AuNPs conjugated with pure phenolics isolated from licorice for the first time. Additionally, we investigate their potential as inhibitors of inflammatory biomarkers.

Inflammation is one of the immune defense mechanisms of organisms when their cells are adversely affected by microbial, physical, or chemical injury [32]. Although inflammation is typically regarded as a vertebrate response to adverse effects, studies have shown that inflammation also occurs in some invertebrates [33]. The adversely affected cells send out chemical messengers, namely inflammatory chemicals and cytokines, to inform the immune system and other cells of the adverse event/s. Several in vitro and in vivo inflammatory messengers or biomarkers have been well characterized, and these include nitric oxide (NO) and the cytokines interleukin 6 (IL-6) and interferon gamma (IFN- γ) [34].

This study is limited to phenolic compounds from licorice and their ability to inhibit inflammatory biomarkers synthesized by the RAW 264.7 macrophage cell line. Previous studies by us and others [35–37] showed that addition of lipopolysaccharides (LPSs) to RAW 264.7 culture medium induced several biomarkers of inflammation, such as nitric oxide, interleukin 6, and tumor necrosis factor. LPSs' addition to cultures also resulted in the upregulation of inducible nitric oxide synthase (iNOS) [38,39].

NO is an important signaling molecule that plays a role in initializing the inflammatory process. NO formation is catalyzed by nitric oxide synthases (NOSs), as these enzymes convert arginine into citrulline via the co-factors oxygen and nicotinamide adenine dinucleotide phosphate (NADPH), with NO being produced during this process. There are three isoforms of NOS, which can be found in a number of tissue and cell types. The three isoforms of NOS are neuronal NOS (nNOS), endothelial NOS (eNOS), and inducible NOS (iNOS) [40]. iNOS is induced via LPS stimulation as LPS acts via the CD14 receptor on the cell membrane and subsequently activates NF κ B, leading to the expression of iNOS and subsequent NO production [41].

2. Materials and Methods

2.1. Materials

2.1.1. Chemicals and Reagents

All solvents used for extraction and column chromatography were general-purpose reagents. Methanol (AR), hexane, dichloromethane, methanol (HPLC grade), ethanol, ethyl acetate, sodium tetrachloroaurate (III) dihydrate ($\text{NaAuCl}_4 \cdot 2\text{H}_2\text{O}$, 99.99%), and glycine (Gly) were purchased from Sigma-Aldrich (Cape Town, South Africa). Polyethylene glycol (PEG), cysteine (Cys), Dulbecco's Modified Eagle (DMEM), and bovine serum albumin (BSA) from Miles Laboratories (Pittsburgh, PA, USA), and *N*-acetyl-L-cysteine from Boehringer Mannheim GmbH (Mannheim, Germany). Polystyrene 96-well microtiter plates were obtained from Greiner Bio-one GmbH (Frickenhausen, BY, Germany). Silica gel 60 (0.063–0.200 mm) and Sephadex (LH-20) were supplied by Merck (Darmstadt, Germany). The murine macrophage cell line, RAW 264.7, was obtained from the American Type Culture Collection (ATCC TIB-71, Manassas, VA, USA).

2.1.2. Equipment

A SPECTROstar Nano (BMG LABTECH, Ortenberg, Germany) 2450 ultraviolet/visible (UV-Vis) spectrophotometer was used to monitor the characteristic peaks of the AuNPs. High-resolution transmission electron microscopy (HRTEM) (FEI Tecnai G2 F20 S-Twin HR-TEM, Hillsboro, OR, USA, operated at 200 kV) was used to study the morphology of the AuNPs. An Oxford energy-dispersive X-ray spectroscopy system inside a Zeiss Auriga Field Emission Scanning Electron Microscope (Miramar, Oxfordshire, UK) was used for elemental analysis. Dynamic light scattering (DLS) analysis was carried out using a Malvern Zetasizer (Malvern Ltd., Malvern, UK) at 25 °C and a 90° angle. A Fourier transform infrared (FTIR) spectrophotometer (Waltham, MA, USA) was used to measure the IR spectra. The 1D NMR (^1H , ^{13}C and DEPT-135) and 2D spectra were measured using a Bruker spectrometer (Rheinstetten, Germany) operating at 400 MHz (for ^1H) and 100 MHz (for ^{13}C).

2.2. Methods

2.2.1. Extraction and Purification of Phenolic Compounds

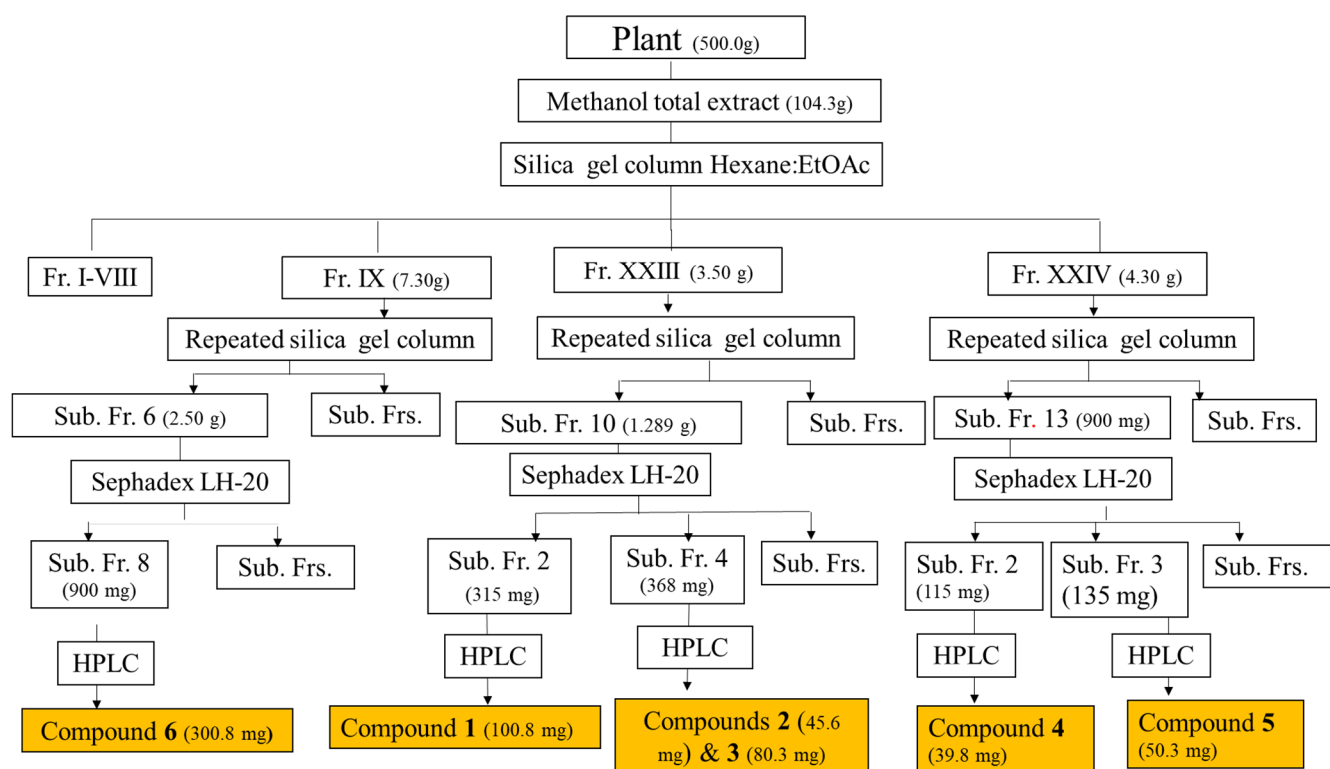
Licorice powder (500.0 g) was extracted with methanol at 60 °C (3 L \times 2 h \times 2 times). After concentration, it yielded 104.3 g. Fifty grams of the total extract (TE) was applied to the silica gel column and eluted with hexane/ethyl acetate gradient of increasing polarity (starting from EtOAc 0% (2L), 10% (2L), 30% (2L), 50% (2L), 80% (2L), and 100 (1L)).

Collected fractions were pooled according to their profiles on the thin layer chromatography (TLC) to afford 24 major fractions coded as I to XXIV. Specific fractions were selected (according to their ability to synthesize NPs) and rechromatographed to yield six major compounds as follows (Scheme 1):

The main fraction XXIII (3.50 g) was chromatographed on silica gel using a gradient of hexane and EtOAc (80:20 to 0:100). The obtained sub-fraction 10 was purified on Sephadex (Merck, Cape Town, South Africa) using isocratic 80% aqueous ethanol then semi-prep HPLC using a gradient of MeOH and DIW (de-ionized water) (40:60 to 60:80 in 30 min, and to 80:90 in 10 min, then to 100% MeOH in 10 min) to give compounds **1** (100.8 mg), **2** (45.6 mg), and **3** (80.3 mg).

The main fraction XXIV (4.30 g) was chromatographed on silica gel. Subfractions 2 and 3 were chromatographed separately on Sephadex and semi-prep HPLC, as previously mentioned, to give compounds **4** (39.8 mg) and **5** (50.3 mg).

The main fraction IX (7.30 g) was chromatographed on silica gel using a gradient of hexane and EtOAc (80:20 to 0:100), and the sub-fraction 6 was purified on Sephadex and then semi-prep HPLC using a mixture of MeOH and DIW (1:1, isocratic) to give compound **6** (300.8 mg). The analysis of the total extract using LC-MS was carried out to profile and identify the compounds associated with nanoparticles when the total extract was used (Supplementary Material Figure S1).



Scheme 1. Schematic diagram for the isolation and purification of the major compounds from licorice, Fr(s). = Fraction(s).

2.2.2. Green Synthesis of Gold Nanoparticles

Total extracts/pure compounds were used to prepare AuNPs: a fresh 16.0 mg/mL stock solution of each extract/pure compound in 50% methanol/distilled water was prepared. Serial dilutions from 2.66 to 0.083 mg/mL were prepared in a 96-well plate. To 50 μ L of the TE/compounds solution, 250 μ L of 0.00125 mM of gold salt was added, and plates were incubated at 60 $^{\circ}$ C. The change of color from light yellow to reddish or purple indicated the successful formation of AuNPs [42]. The optimum concentrations were selected to scale up the AuNPs' preparation to obtain enough material for biological studies. The formation of the AuNPs was further confirmed by recording a UV-vis spectrum in the 300–800 nm range [43].

2.2.3. Characterization of Gold Nanoparticles

Different characterization techniques such as UV-vis, HRTEM, FTIR, and DLS were used to investigate the formation of AuNPs and their various physicochemical properties. The absorption bands due to electrons confined on the surface were measured using a microtitre plate reader (BMG Labtech, Ortenberg, Germany). Zeta potential, hydrodynamic size, and polydispersity indices (Pdis) were measured using Malvern Zetasizer. HRTEM images were analyzed using ImageJ software, 1.50b version 1.8.0_60 (<http://imagej.nih.gov/ij> (accessed on 17 May 2022)) and Origin pro-2022b (64 bits) software, respectively. Vibrational bands of possible functional groups of the synthesized AuNPs were recorded on FTIR at a 400–4000 cm^{-1} transmission mode.

2.2.4. Stability Study

The method described by Elbagory et al. in 2016 was utilized [31]. Briefly, 100 μ L of the AuNP solutions were incubated with equal volume (1:1) of the buffer solutions BSA, PBS, PEG, Gly, and Cys) in a 96-well plate. The final concentrations of the biological media in the final mixture were as follows: 5% PEG, 0.5% cysteine, glycine, PBS, and 0.5% BSA.

The stability of the AuNPs was evaluated by measuring the changes in the UV–vis spectra after 24 h.

2.2.5. Biological Study

Preparation of Stock Solutions

AuNP conjugates, total methanolic extract, and pure compounds were reconstituted in DMSO. After that, a 1.2 mg/mL stock solution of the relevant treatment (AuNP conjugates, total methanolic extract, and pure compounds) was prepared in sterile distilled water. Before cell exposure, the stock solutions were briefly sonicated (QSonica, LLC. Misonixsonicators, XL-200 Series, Newtown, CT, USA) on ice for approximately 3 min. After that, the stock solutions were further diluted in complete Dulbecco's Modified Eagle's Medium (DMEM, Lonza, Cape Town, South Africa). Complete DMEM consisted of 10% heat-inactivated fetal bovine serum (FBS, Life Technologies ThermoFisher Scientific, Bedford, MA, USA), 1% antibiotic/antimycotic solution, 1% glutamax, and 0.5% gentamicin (Sigma-Aldrich, St. Louis, MO, USA).

Cell Culture and Exposure

Cells were cultured in complete DMEM, incubated at 37 °C in a humidified atmosphere of 5% CO₂, and sub-cultured every 2–3 days.

The RAW 264.7 cells were seeded at 1×10^6 cells/mL in 96-well tissue culture-treated plates for cell viability and nitric oxide assays. The seeded cells were incubated under standard tissue culture conditions at 37 °C in a humidified atmosphere of 5% CO₂ for approximately 24 h until the cells reached 70–80% confluence. The cells were subsequently exposed to the relevant AuNP conjugates, total extract, or compounds. After that, the cells were either left unstimulated or stimulated with 1 µg/mL lipopolysaccharide (LPS, from *E. coli* O111:B4, Sigma-Aldrich) to yield a final concentration range of 0–100 µg/mL of the appropriate treatment. The cells were then incubated overnight under standard tissue culture conditions.

Cell Viability Assay

The supernatants were removed after incubation, and cells were washed with phosphate-buffered saline (PBS, Lonza). Cell viability was assessed by adding 50 µL of a 1/10 dilution of 2-(4-iodophenyl)-3-(4-nitrophenyl)-5-(2,4-disulfophenyl)-2H-tetrazolium (WST-1, Roche, Basel, Switzerland) in complete DMEM medium to each well. Metabolically active cells convert the WST-1 reagent to a formazan that can be measured spectrophotometrically. Formazan formation was determined by reading the plate at 450 nm immediately after adding WST-1 and again after an incubation period of 1 h at 37 °C. The increase in absorbance is proportional to formazan formation and directly proportional to cell viability. The difference between the zero-absorbance reading and 1 hr incubation was used to calculate the percentage of cell viability. Cell viability was calculated as a percentage of the control using the below formula:

$$\text{Cell viability as a \% of Control} = \frac{T1 - T0}{U1 - U0} \times 100 \quad (1)$$

where T1 is the absorbance of the treated sample after 1 h, T0 is the absorbance of the treated at 0 h, U1 is the absorbance of the untreated sample after 1h, and U0 is the absorbance of the untreated sample at 0 h.

Nitric Oxide (NO) Assay

In the initial development of the assay, polymyxin inhibition of LPS inflammatory activity was checked. Polymyxin was established to inhibit LPS-induced inflammatory activity in macrophage cultures [37]. Cell culture supernatants were removed after the overnight incubation with the relevant treatment. They were used to determine the amount of nitrite produced by the cells and used as an indication of NO production. The amount of

NO produced was determined against a 0–100 μM nitrite standard range (Sigma-Aldrich). Culture supernatants or nitrite standard (50 μL) were mixed with 50 μL of Griess reagent (Sigma-Aldrich). The absorbance was subsequently read spectrophotometrically at 540 nm (Multiskan Ex, Thermo Electron Corporation, Vantaa, Finland), and the amount of NO produced by the cells was quantified. NO levels were not determined at cytotoxic concentrations.

2.3. Statistical Analysis

All experiments were performed in triplicate, and the data were calculated using Microsoft Excel. Data are represented as the mean \pm standard error of the mean (SEM). Statistical differences with $p < 0.001$ were deemed significant after conducting a one-way analysis of variance (ANOVA) using Sigma Plot 12.0 (Systat Software Inc., San Jose, CA, USA).

3. Results

3.1. Chemical Characterization of the Isolated Compounds

Chromatographic purification of the total extract using different techniques, including HPLC (Scheme 1), resulted in the isolation of six pure major compounds, namely, liquiritin (1), isoliquiritin (2), neoisoliquiritin (3), isoliquiritin apioside (4) [44], liquiritin apioside (5), and glabridin (6) [45]. The compounds (Figure 1) were identified based on detailed spectroscopic analysis (Figure S2.1–S2.6 and Table 1) and comparison with the reported data [46].

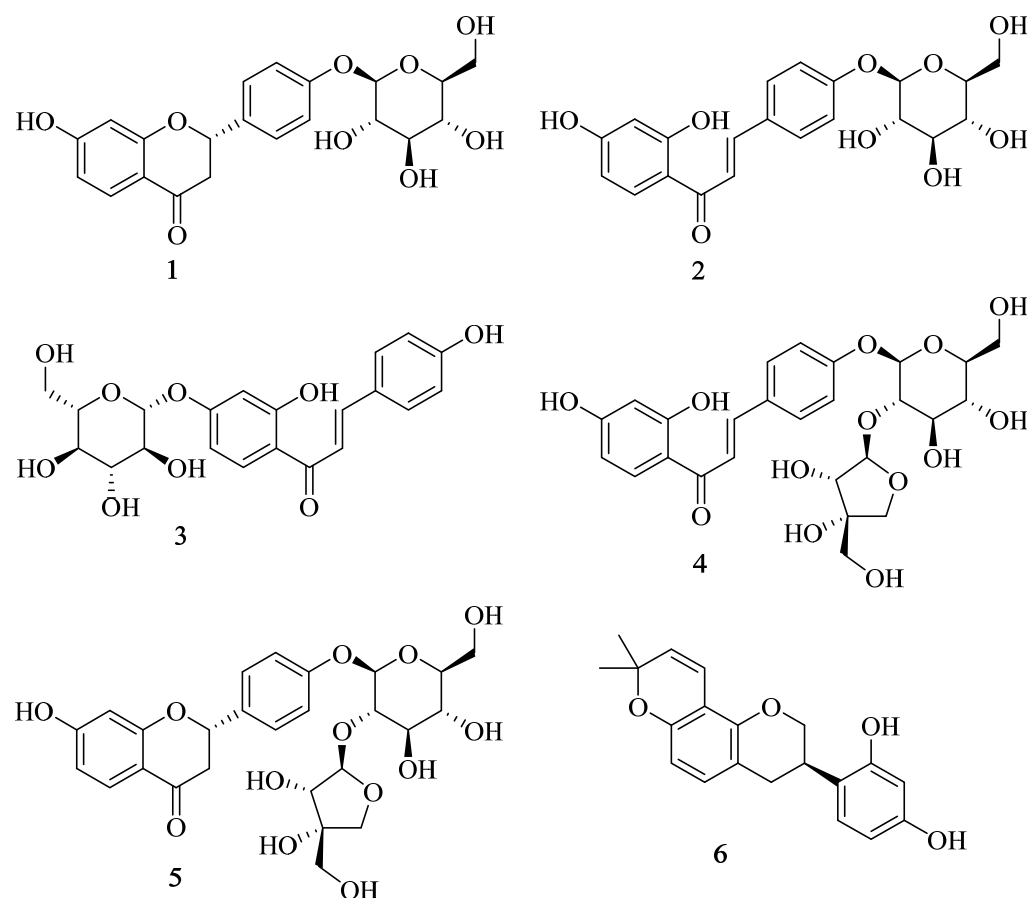


Figure 1. The chemical structures of the isolated compounds (1–6) from licorice.

Table 1. ¹H and ¹³C NMR spectroscopic data for compounds 1–6*.

Liquiritin (1)		Liquiritin Apioside (5)		Glabridin (6)		Isoliquiritin (2)		Neoisoliquiritin (3)		Isoliquiritin Apioside (4)			
d _C	d _H (multi, J)	d _C	d _H (multi, J)	d _C	d _H (multi, J)	d _C	d _H (multi, J)	d _C	d _H (multi, J)	d _C	d _H (multi, J)		
1	-	-	-	-	-	C=O	191.7	-	192.5	-	191.1	-	
2	78.6	5.52 (br d, 13.0)	78.9	5.51 (d, 2.0, 13.0)	70.02	4.20 (d, 10.0) 3.85 (d, 10.0)	α	119.6	7.87 (d, 15.5)	117.7	7.82 (d, 16.6)	119.2	7.86 (d, 15.8)
3	43.2	3.12 (dd, 16.6, 13.0) 2.66 (br d, 16.6)	43.1	3.11 (dd, 16.0, 13.0) 2.26 (br d, 16.0)	31.60	3.33 m	β	143.8	7.77 (d, 15.5)	145.5	7.79 (d, 16.6)	143.2	7.76 (d, 15.8)
4	189.9	-	189.9	-	30.36	2.64 (d, 15.3) 2.84 (dd, 3.1, 15.3)	1	133.4	-	125.9	-	128.4	-
5	128.4	7.63 (d, 8.6)	128.1	7.64 (d, 9.0)	127.8	6.15 (d, 8.2)	2	128.8	7.86 (d, 8.8)	132.9	7.79 (d, 8.4)	130.7	7.86 (d, 8.8)
6	110.8	6.36 (d, 2.0)	110.8	6.51 (dd, 9.0, 1.2)	109.5	6.69 (d, 8.2)	3	116.9	7.10 (d, 8.8)	116.4	6.85 (d, 8.4)	116.3	7.07 (d, 8.8)
7	165.2	-	165.1	-	151.8	-	4	159.8	-	161.2	-	159.2	-
8	102.6	6.51 (d, 2.0, 8.6)	102.6	6.35 (d, 1.2)	106.8	-	5	116.9	7.10 (d, 8.8)	116.4	6.85 (d, 8.4)	116.3	7.07 (d, 8.8)
9	163.1	-	163.1	-	149.7	-	6	128.8	7.86 (d, 8.8)	131.9	7.78 (d, 8.4)	130.7	7.86 (d, 8.8)
10	113.3	-	113.3	-	114.7	-	1'	113.2	-	115.2	-	112.6	-
1'	132.4	-	132.4	-	118.3	-	2'	166.3	-	163.9	-	165.9	-
2'	128.0	7.44 (d, 8.6)	128.4	7.44 (d, 8.5)	155.9	-	3'	103.0	6.25 (d, 1.7)	103.9	6.58 (d, 1.8)	102.6	6.28 (d, 2.0)
3'	116.2	7.06 (d, 8.5)	116.0	7.04 (d, 8.5)	102.6	6.33 (d, 2.3)	4'	166.3	-	165.6	-	165.9	-
4'	157.4	-	157.3	-	157.1	-	5'	108.9	6.41 (dd, 1.7, 9.0)	108.6	6.62 (dd, 1.8, 9.0)	108.6	6.25 (d, 2.0)
5'	116.2	7.06 (d, 8.5)	116.0	7.04 (d, 8.5)	108.3	6.14 (dd, 2.3, 8.4)	6'	131.2	8.18 (d, 9.0)	131.9	8.27 (d, 9.0)	132.9	8.17 (d, 9.0)
6'	128.0	7.44 (d, 8.6)	128.1	7.44 (d, 8.5)	128.7	6.81 (d, 8.4)	1''	100.3	4.98 (d, 8.8)	100.0	5.04 (d, 8.6)	98.3	5.05 (d, 7.4)
1''	100.3	4.89 (d, 7.3)	98.6	4.96 (d, 7.2)	116.8	6.48 (d, 9.8)	2''	73.6	3.29 (d, 8.6)	73.5	3.24 (d, 7.4)	79.3	3.74 (br s)
2''	73.2	3.26 ^a (m)	75.7	3.74 (s)	129.2	5.47 (d, 9.8)	3''	77.0	3.30 (t, 8.6)	76.9	3.31 (t, 9.0)	76.9	3.49 ^a
3''	77.0	3.33 ^a	77.1	3.36 ^a	75.1	-	4''	70.1	3.17 (t, 8.8)	70.0	3.17 (t, 8.4)	69.9	3.19 (t, 7.5)
4''	69.7	3.17 (dd, 8.9, 10.0)	69.9	3.95 (d, 9.4)	26.6	1.23 (s)	5''	77.6	3.34 (dd, 9.4, 7.6)	77.6	3.34 (dd, 9.0, 7.0)	77.1	3.42 ^a
5''	76.6	3.28 ^a	76.9	3.49 ^a	26.6	1.23 (s)	6''	61.1	3.69 (d, 11.0) 3.18 (dd, 8.0, 11.0)	61.0	3.69 (d, 11.0) 3.34 (dd, 11.0, 7.0)	60.5	3.45 ^a 3.70 (br d, 10.9)
6''	60.7	3.69 (d, 11.4) 3.47 (dd, 5.5, 11.4)	60.6	3.45 ^a 3.69 (br d, 11.6)	-	-	1'''	-	-	-	108.6	5.36 (br s)	
1'''	-	-	108.7	5.36 (s)	-	-	2'''	-	-	-	76.0	3.51 (d, 7.4)	
2'''	-	-	77.6	3.48 ^a	-	-	3'''	-	-	-	79.3	-	
3'''	-	-	79.3	-	-	-	4'''	-	-	-	74.0	3.65 (d, 9.5) 3.94 (d, 9.5)	
4'''	-	-	74.0	3.65 (d, 9.3) 3.94 (d, 9.3)	-	-	5'''	-	-	-	64.3	3.31 (s, 2H)	
5'''	-	-	64.3	3.33 (s, 2H)	-	-	-	-	-	-	-	-	

* Spectra were measured in DMSO-*d*₆ except compound (6) in acetone. NMR operated at 400 MHz (¹H) and 100 MHz (¹³C), *multi*: multiplicity, *J* values in Hz, *s* singlet, *br s* broad singlet, *d* doublet, *dd* doublet of doublet, *br d* broad doublet, *t* triplet, *m* multiple; ^a overlapped signals in the same column.

3.2. Preparation and Characterization of AuNPs

At the outset, the total extract exhibited promising potential for forming AuNPs. Subsequently, through a phytochemical process, we isolated six major compounds with significant reducing capabilities, which were then utilized for the green synthesis of AuNPs. The synthesized nanoparticles underwent characterization using various spectroscopic techniques, including ultraviolet–visible (UV–vis) (see Figure S3 and Table 2) [13], particle size and zeta potential (Zp) measurement (see Table 2 and Figure S4), high-resolution transmission electron microscopy (HRTEM) (see Table 2 and Figure S5), X-ray diffraction (XRD) [47] (see Figure S8 and Table 2), and Fourier transform infrared (FTIR) spectroscopy [43] (see Figures S9 and S10).

Table 2. Particle sizes, zeta potential, polydispersity index, UV absorbance, and HRTEM average size measurements of different synthesized AuNPs.

Sample	Zeta Potential (mV)	Pdi	Hydrodynamic Size (nm)	UV–Vis λ Max (nm)	Average Size from XRD * (nm)
1@AuNPs	−29.9	0.12	184.0	551	6.56
2@AuNPs	−20.2	0.26	221.9	547	5.48
3@AuNPs	−32.3	0.12	351.0	550	10.02
4@AuNPs	−9.10	0.22	184.0	553	9.24
5@AuNPs	−17.1	0.34	79.31	556	10.06
6@AuNPs	−32.7	0.19	257.8	544	10.02
TE@AuNPs	−27.7	0.23	320.0	538	10.06

* Values obtained using the Scherrer equation (see Table S1).

3.3. Stability Study

The stability of nanoparticles in biological media has different durations depending on the type of nanoparticle. The stability study was carried out in various media, including bovine serum albumin (BSA), phosphate-buffered saline (PBS), polyethylene glycol (PEG), glycine (Gly), and cysteine (Cys). The media were added (1:1, *v/v*) to the synthesized AuNPs. These were placed in a 96-well plate and incubated at 37 °C for different periods. UV–vis monitored the stability for a period of 24 h (Figures S6 and S7).

3.4. Biological Activity of AuNPs

Inflammation is a host response to harmful stimuli and features traditional signs such as redness, swelling, heat, and pain. This study aimed to assess the activity of the crude extract, pure compounds, and their nanoparticles on NO production [29,30].

3.4.1. Cell Viability

RAW cell viability in the presence of the extract, compounds, and nanoparticles was determined using the WST-1 assay in unstimulated and LPS-stimulated conditions (Table 3). Cell viability indicates whether a specific additive to cultured cells activates or reduces the number of viable cells and usually is indirectly proportional to the toxicity of the additive.

Table 3. Approximate cell viability IC₅₀ values ($\mu\text{g/mL}$) of the respective compounds and their AuNPs conjugates \pm SEM.

Sample	−LPS		+LPS	
	Comp.	AuNP	Comp.	AuNP
Comp. 1	39.7 \pm 1.6	-	60.5 \pm 4.5	-
Comp. 2	-	29.2 \pm 2.3	-	-
Comp. 3	-	-	-	-
Comp. 4	-	-	-	-
Comp. 5	47.8 \pm 0.2	33.7 \pm 2.5	-	-
Comp. 6	28.4 \pm 6.5	38.2 \pm 4.1	27.2 \pm 1.5	35.5 \pm 2.1
TE	-	-	-	-

3.4.2. Liquiritin (1) and Liquiritin Conjugated to AuNPs (1@AuNPs)

Under a simulated inflammatory response, RAW cells experienced a significant ($p < 0.001$) loss of viability at 50 $\mu\text{g/mL}$ AuNPs (Figure 2a). In comparison, compound 1 was cytotoxic at concentrations of 50–100 $\mu\text{g/mL}$ in the absence and presence of LPS, with approximate IC_{50} values of 39.7 ± 1.6 and 60.5 ± 4.5 $\mu\text{g/mL}$, respectively (Table 3).

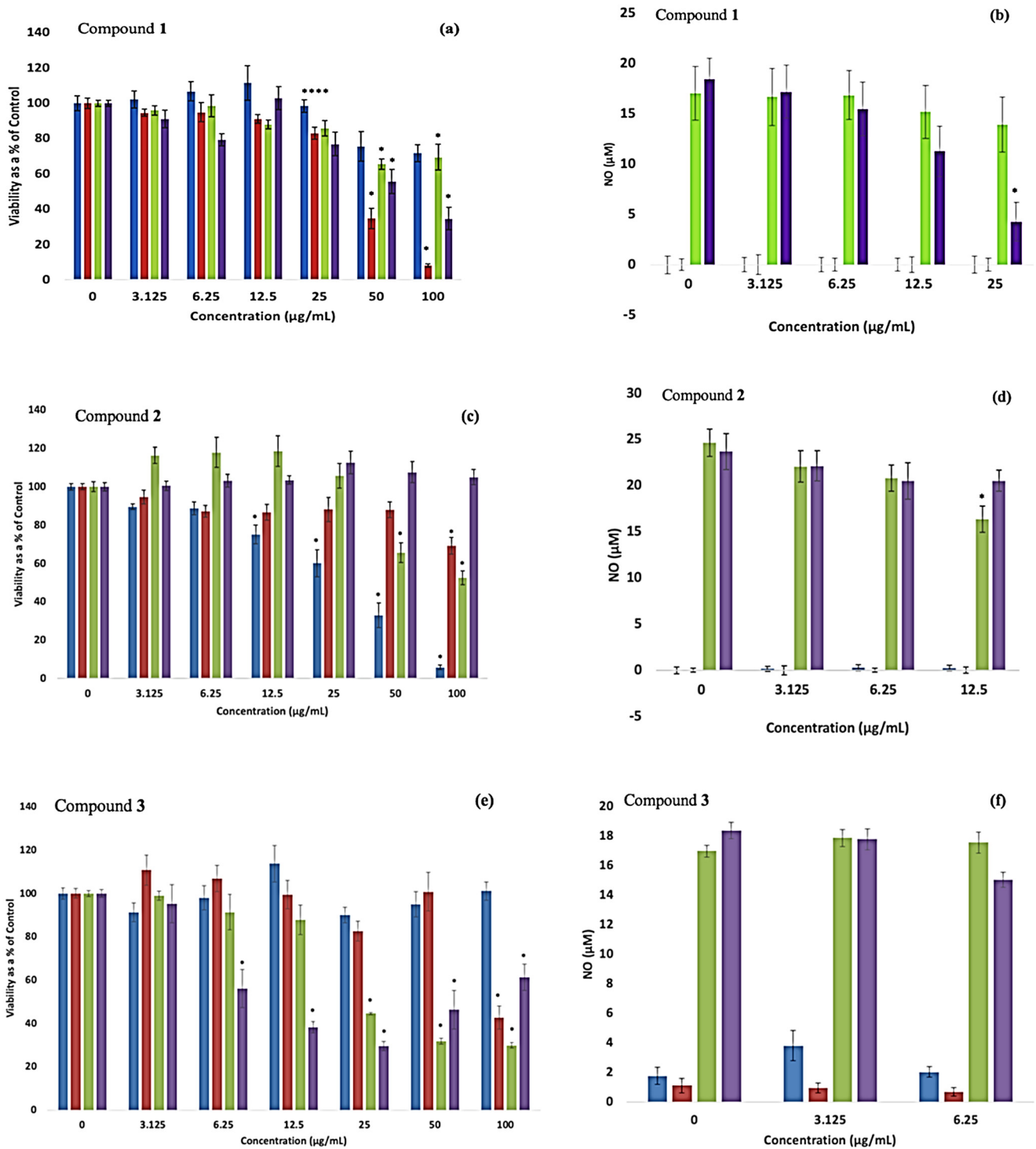


Figure 2. Cont.

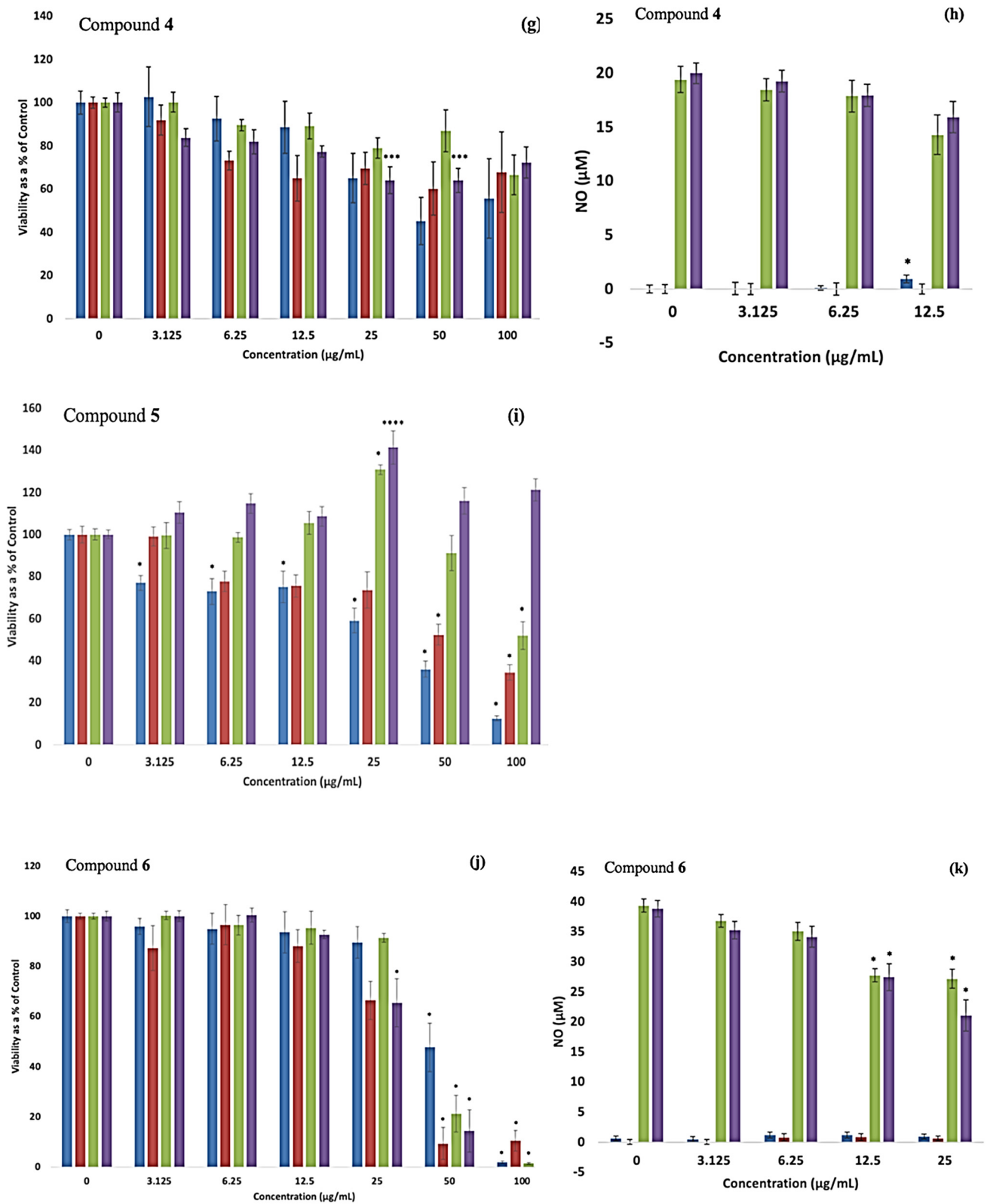


Figure 2. Cont.

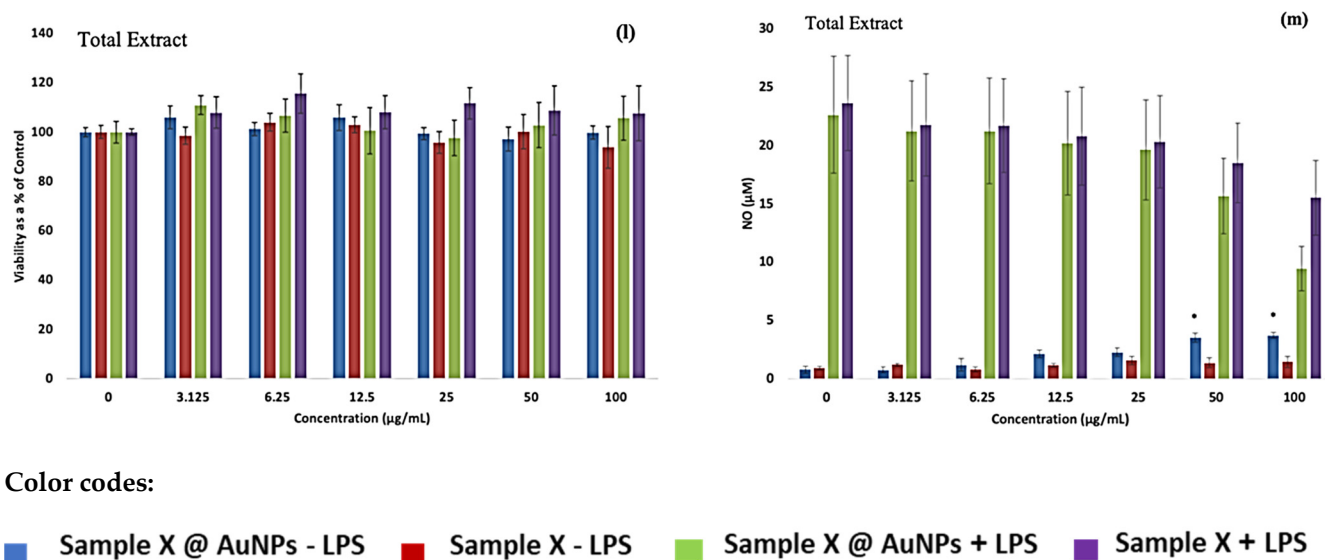


Figure 2. The assessment of RAW 264.7 cell viability and NO after 24 h exposure to various AuNPs, TE, and compounds in either the presence or absence of LPS. Cells were treated with the following: (a,b) compound 1; (c,d) compound 2; (e,f) compound 3; (g,h) compound 4; (i) compound 5; (j,k) compound 6; (l,m) TE. Data are presented as mean \pm SEM, where the *p*-value indicates statistical significance against the relevant control, using one-way ANOVA. * *p* < 0.001, *** *p* = 0.003, and **** *p* = 0.005. Sample X + LPS and green should be Sample X + AuNPs + LPS.

3.4.3. Isoliquiritin (2) and 2@AuNPs

The AuNPs in the absence of LPS significantly (*p* < 0.001) decreased RAW cell viability at concentrations ≥ 12.5 $\mu\text{g}/\text{mL}$ (Figure 2c), with the cell viability ranging from 75–5%, ($\text{IC}_{50} \sim 29.2 \pm 2.3$ $\mu\text{g}/\text{mL}$) (Table 2). However, a mitogenic effect was seen in the presence of LPS as the AuNPs induced significant (*p* < 0.001) cytotoxicity only at concentrations of 50 $\mu\text{g}/\text{mL}$, ranging from 65–8% viability. A noticeable (*p* < 0.001) drop in viability was seen only at 100 $\mu\text{g}/\text{mL}$ of compound 2 under basal conditions, and no cytotoxicity was exhibited under a simulated inflammatory response.

3.4.4. Neoisoliquiritin (3) and 3@AuNPs

The AuNPs did not affect RAW cell viability across the concentration range assessed in the absence of LPS (Figure 2e). Conversely, in the presence of LPS, the AuNPs significantly (*p* < 0.001) decreased cell viability at concentrations ≥ 25 $\mu\text{g}/\text{mL}$. In the absence of LPS, compound 5 reduced (*p* < 0.001) cell viability to 40% only at the highest exposed concentration (100 $\mu\text{g}/\text{mL}$). In contrast, compound 5 in the presence of the mitogen LPS reduced (*p* < 0.001) cell viability by approximately 40% at concentrations ≥ 6.25 $\mu\text{g}/\text{mL}$.

3.4.5. Isoliquiritin Apioside (4) and 4@AuNPs

RAW cells exposed to the pure compound significantly (*p* = 0.003) reduced viability to 60 and 70% when exposed to 25 and 50 $\mu\text{g}/\text{mL}$ in the presence of LPS (Figure 2g). The pure compound did not affect cell viability without LPS. AuNPs did not exert any detrimental effects on cell viability, regardless of the absence or presence of LPS.

3.4.6. Liquiritin Apioside (5) and 5@AuNPs

The AuNPs under basal conditions noticeably reduced (*p* < 0.001) cell viability in a dose-dependent manner at all concentrations assessed in the study (Figure 2i). Conversely, when stimulated with LPS, the nanoparticles exhibited a mitogenic effect, increasing (*p* < 0.001) cell viability at 25 $\mu\text{g}/\text{mL}$. They reduced (*p* < 0.001) viability only at 100 $\mu\text{g}/\text{mL}$. Without LPS, compound 5 significantly (*p* < 0.001) reduced viability by 40% at concentrations ≥ 50 $\mu\text{g}/\text{mL}$, with an approximate IC_{50} of 33.7 ± 2.5 $\mu\text{g}/\text{mL}$ (Table 2). Exposure

to compound **5** in the presence of LPS did not negatively impact cell viability, instead increasing ($p = 0.005$) cell viability at 25 $\mu\text{g/mL}$.

3.4.7. Glabridin (**6**) and **6@AuNPs**

The AuNPs exhibited a noticeable ($p < 0.001$) decrease in cell viability at concentrations $\geq 50 \mu\text{g/mL}$ in both the unstimulated and LPS-stimulated conditions (Figure 2j), with approximate IC_{50} values of 38.2 ± 4.1 and $35.5 \pm 2.1 \mu\text{g/mL}$, respectively (Table 2). The percentage of viable cells was identified as 30% at concentrations of AuNPs $\geq 50 \mu\text{g/mL}$. The unstimulated pure compound also produced a significant ($p < 0.001$) loss of viability at concentrations $\geq 50 \mu\text{g/mL}$, with the percentage of viable cells $\leq 30\%$ ($\text{IC}_{50} \sim 28.4 \pm 6.5 \mu\text{g/mL}$). The LPS-stimulated compound **6** was cytotoxic ($p < 0.001$) at $\geq 25 \mu\text{g/mL}$ concentrations, with percentage viability ranging from 65 to 9%, respectively ($\text{IC}_{50} \sim 27.2 \pm 1.5 \mu\text{g/mL}$).

3.4.8. Total Extract (TE) and TE@AuNPs

When exposed to the cells, all the experimental concentrations of the extract and NP were not cytotoxic (0–100 $\mu\text{g/mL}$) (Figure 2l).

To summarize, the AuNPs conjugated with isoliquiritin apioside (**4**) were not toxic to the RAW cells across the concentration range in the presence or absence of LPS. Similarly, the TE alone was not toxic under all conditions and all the exposure concentrations. Comparably, the compounds liquiritin apioside (**5**) and isoliquiritin (**2**) did not hinder cell proliferation in the presence of LPS.

The RAW cells exposed to the pure compounds in the absence of LPS experienced different cytotoxic sensitivities: liquiritin (**1**) > liquiritin apioside (**5**) > glabridin (**6**) > neoisoliquiritin (**3**) > isoliquiritin (**2**). However, in the presence of LPS, the sensitivity of RAW cell viability differed from that of the unstimulated data. These sensitivities were neoisoliquiritin (**3**) > glabridin (**6**) > isoliquiritin apioside (**4**) > liquiritin (**1**).

The viability of the RAW cells was sensitive to three of the seven AuNPs in the absence of LPS: **5@AuNPs** > **2@AuNPs** > **6@AuNPs**. In the presence of LPS, the cells were sensitive to **3@AuNPs** > **2@AuNPs** > **6@AuNPs** > **1@AuNPs** > **5@AuNPs**.

3.5. Nitric Oxide Production

The NO assay based on the Griess reaction was used to assess the production of NO from the RAW cells after the exposure to the NP extract/pure compounds in either the absence or presence of LPS.

3.5.1. Liquiritin (**1**) and **1@AuNPs**

Compound **1** and **1@AuNPs** did not elicit NO secretion from the RAW cells without LPS (Figure 2b). An anti-inflammatory response was seen when the cells were exposed to compound **1** in the presence of LPS. Compound **1** reduced ($p < 0.001$) the inflammatory activity at 25 $\mu\text{g/mL}$, with an approximate IC_{50} value of $16.5 \pm 1.4 \mu\text{g/mL}$ (Table 4).

Table 4. Approximate NO IC_{50} values ($\mu\text{g/mL}$) of the respective compounds and their AuNPs conjugates \pm SEM.

Sample	−LPS		+LPS	
	Comp.	AuNP	Comp.	AuNPs
Comp. 1	-	-	16.5 ± 1.4	-
Comp. 2	-	-	-	18.2 ± 0.8
Comp. 3	-	-	-	-
Comp. 4	-	-	-	-
Comp. 5	-	-	-	-
Comp. 6	-	-	27.5 ± 1.5	-
TE	-	-	-	-

3.5.2. Isoliquiritin (2) and 2@AuNPs

RAW cells challenged with LPS, 2@AuNPs reduced ($p < 0.001$) the inflammatory activity at 12.5 $\mu\text{g}/\text{mL}$ (Figure 2d), with an $\text{IC}_{50} \sim 18.2 \pm 0.8 \mu\text{g}/\text{mL}$ (Table 4). Compound 2 and 2@AuNPs under basal conditions did not affect the level of NO secreted by the cells.

3.5.3. Neoisoliquiritin (3) and 3@AuNPs

The 3@AuNPs and compound in the presence or absence of LPS did not affect the level of NO secreted from the RAW cells (Figure 2f).

3.5.4. Isoliquiritin Apioside (4) and 4@AuNPs

Isoliquiritin apioside under basal conditions did not elicit an inflammatory response from the RAW cells (Figure 2h). The AuNPs at basal levels induced ($p < 0.001$) NO production at 12.5 $\mu\text{g}/\text{mL}$. In the presence of LPS, compound 4 and 4@AuNP did not impact NO secretion from the RAW cells.

3.5.5. Liquiritin Apioside (5) and 5@AuNPs

The level of NO secreted from the cells was not evaluated as 5@AuNP was shown to be cytotoxic (Figure 2i).

3.5.6. Glabridin (6) and 6@AuNPs

The AuNPs and the pure compound did not affect NO production without LPS (Figure 2k). However, in the presence of LPS, both the AuNPs and compound 6 reduced ($p < 0.001$) the production of NO from the RAW cells at concentrations $\geq 12.5 \mu\text{g}/\text{mL}$, indicating anti-inflammatory activity. Compound 6 exhibited an approximate IC_{50} value of $27.5 \pm 1.5 \mu\text{g}/\text{mL}$ in the presence of LPS (Table 4).

3.5.7. Total Extract (TE) and TE@AuNPs

The TE-capped AuNPs induced an inflammatory response ($p < 0.001$) under basal conditions at concentrations $\geq 50 \mu\text{g}/\text{mL}$ (Figure 2m). This increase in NO production was seven times more than that of the negative control (0 $\mu\text{g}/\text{mL}$ -LPS). TE@AuNPs did not impact NO production in the presence of LPS. The production of NO was not affected by the TE in either the absence or presence of LPS.

Without LPS, neither the TE nor any of the pure compounds affected NO secretion. In the absence of LPS, NO secretion was modulated by the TE@AuNPs and 4@AuNPs. In the presence of LPS, the TE did not affect NO secretion. However, the pure compounds liquiritin (1) and glabridin (6) inhibited NO secretion in the presence of LPS. The NO secretion in the presence of LPS was inhibited by all the compounds conjugated to AuNPs, except liquiritin (1), neoisoliquiritin (3), isoliquiritin apioside (4), and the TE.

The anti-inflammatory potential of the compounds ranged within the order liquiritin (1) \leq glabridin (6) in the presence of LPS. The anti-inflammatory potential of the compounds conjugated to the AuNPs ranged within the order 4@AuNPs \leq TE@AuNPs in the absence of LPS, and 1@AuNPs \leq 6@AuNPs \leq 2@AuNPs in the presence of LPS.

4. Discussion

The synthesis of metal NPs using biological materials, mainly plant extracts, is widely accepted as an eco-friendly method to avoid more contamination of the environment. AuNPs show excellent safety margins and low toxicity in vitro and in vivo, allowing a wide range of applications in the biomedical field.

Plant extracts are a complex mixture of chemical molecules of different natures and functionalities. In the context of metallic NP preparation, total plant extracts are less preferable due to the complex nature of the multicomponent capping surrounding the metal core. Employing a single-molecule approach, particularly in medical applications, is highly recommended as it offers superior advantages.

Natural compounds have a positive impact on human health. When utilized as capping agents, these natural products not only reduce the metal precursors into their metallic form but also enhance the stability and longevity of the resulting metal NPs. Furthermore, employing natural products as capping agents confers additional advantages, such as improved targeting capabilities of AuNPs towards specific tissues or organs, thus enhancing their smartness. During the process of nanoparticle formation, only a small portion of the active compound(s) undergoes conjugation in the nanoform. Despite this conjugated form having a lower concentration, it has been reported to exhibit enhanced activity compared with the intact extract and active compound(s). Additionally, AuNP conjugates serve as excellent compositions to enhance the bioavailability of natural compounds while mitigating their potential toxicity [48,49].

In this work, six major compounds from licorice were isolated and used as reducing, capping, and stabilizing agents for AuNPs. The SPR bands of the prepared AuNPs ranged between 538–556 nm (Figure S3 and Table 2). The values are within the acceptable published results for AuNPs; for example, mangiferin- and hypoxoside-capped AuNPs' SPR bands were 527 and 534 nm, respectively [17,50].

The ZP of the particles ranged from -9.1 (for 4@AuNPs) to -32.7 mV (6@AuNPs), as indicated (Table 2); compound 6 conjugated AuNPs were the most stable, followed by 3@AuNPs (-32.3), then 1@AuNPs (-29.9). The observation of the low stability of 5@AuNPs (-17.1 mV) compared with 1@AuNPs (-29.9 mV) is interesting since compound 5 is more hydrophilic with one sugar unit extra; the same behavior was also observed between 2@AuNPs (-20.2) and 4@AuNPs (-9.1). Currently, we lack a precise explanation for this behavior, apart from attributing it to the steric effect caused by the presence of bulky sugar units in the case of 4@AuNPs and 5@AuNPs. It is plausible that these bulky groups impede interactions on the metal surface and/or hinder the charge transfer to the capping layers around the core of the metal nanoparticles (NPs). This proposal partially supports the stability observed in the case of 6@AuNPs, which features 6 as the aglycone, devoid of such bulky sugar units [45]. On the other hand, the hydrodynamic size supports the proposed explanation, where the size of 1@AuNPs (184.0 nm) > 5@AuNPs (79.31 nm) and 2@AuNPs (221.9 nm) > 4@AuNPs (184.0 nm).

The TEM analysis (Figure S5) showed comparable small sizes for all samples. These results indicate the fast electron donation of the compounds during the reduction process. TEM analysis also showed polymorphism of all AuNPs formed, and different shapes appeared in the figures. The size variation of the AuNPs can be attributed to the different interaction modes of the phenolics during the reducing and stabilization steps. Polyhydroxylated natural compounds, especially polyphenols, are well known for this behavior under neutral conditions; for example, AuNPs conjugated with mangiferin [14], quercetin [15], proanthocyanidin dimer [16], hypoxoside [17,18], and hesperidin [19,20] showed polymorphic nature.

The XRD pattern (Figure S8) indicated that the biosynthesized gold nanoparticles were crystalline. The average particle size was calculated from the XRD peaks by applying the Scherrer equation. The relative sizes had a range of 5.48–10.06 nm.

It is important to note that the sizes of AuNPs nanoparticles obtained via different methods varied. The DLS method produced a size range of 79 to 350 nm, while HRTEM yielded a range of 16 to 83 nm (Figure S5) and XRD indicated a range of 5 to 10 nm (see Table 2). DLS measurements consider the hydrodynamic size, including the capping agent shells around the metal core, which can introduce errors in determining the actual average particle size. These errors can be up to five times larger than those from TEM. HRTEM measures the actual size related to the metal core of the nanoparticle, but it has the limitation of not necessarily representing the entire population of nanoparticles since the selected image may not be representative. The most accurate method for determining relative particle sizes is through XRD. On the other hand, DLS demonstrates the ability of the metal core to attract more molecules from the surrounding medium, which could

contribute to the payload, bioactivity, and stability of the nanoparticles. Figure 3 shows the possible mechanism of formation of NPs, using chalcone pharmacophore as an example.

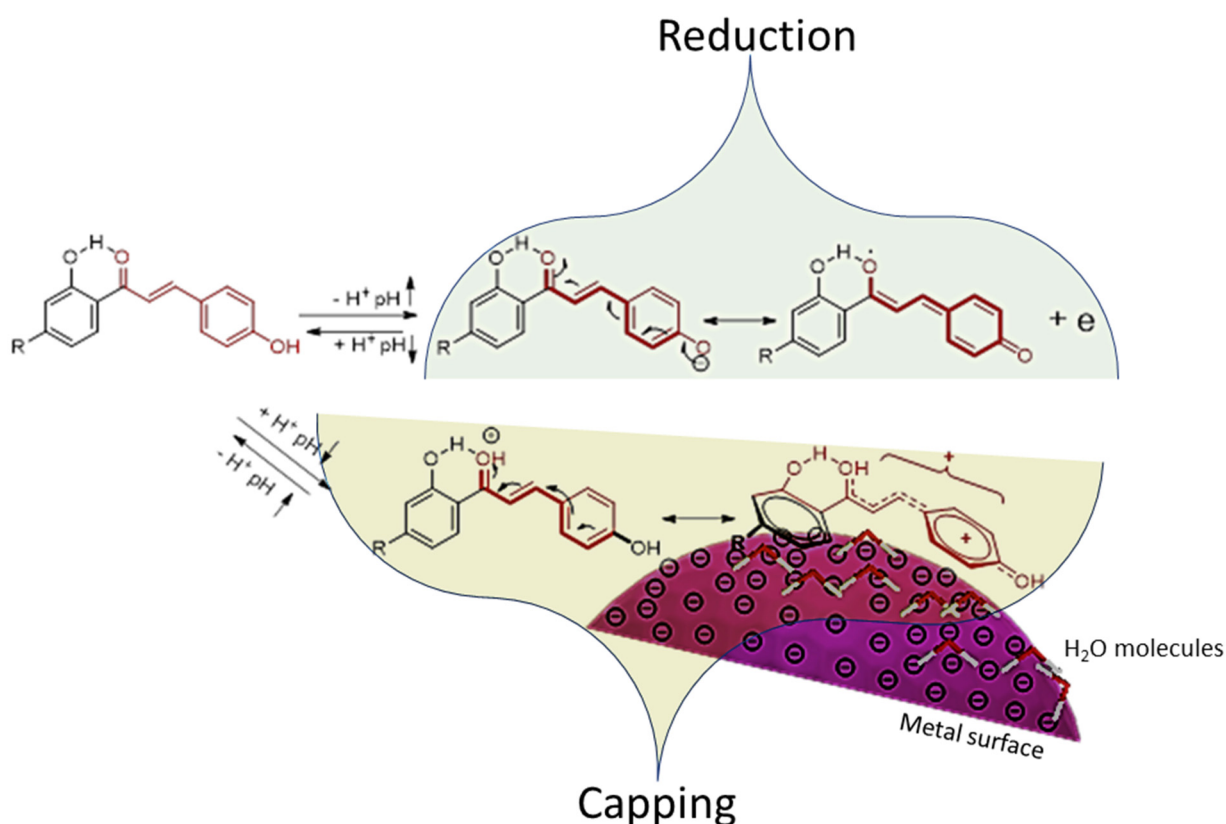


Figure 3. A proposed mechanism for the reduction and capping of chalcones isolated in this study (represented by compound 3). The reduction process includes the loss of an electron and this step is pH-dependent. The second step is the capping process where the compound forming a shell may be two or three layers around the metal NPs.

Figures S9 and S10 show the typical FTIR spectra of each compound with the corresponding AuNPs. Some synthesized AuNPs showed similarities with their respective compounds, confirming the capping agent's presence around the metal NP core [51].

Significantly, it should be noted that the FTIR spectra of compounds 2 and 4 (and their NPs) exhibit similarity due to their shared pharmacophore. The only difference exists in the glycosidic side chain, which has a minimal impact on the characteristics of both compounds. An analogous scenario also applies to compounds 1 and 5.

The stability study of the formed AuNPs is essential to understanding the expected potency and the shelf life of the synthesized AuNPs in different biogenic media. Most of the NPs, notably 4@AuNPs, 5@AuNPs, 6@AuNPs, and TE@AuNPs, demonstrated stable color across various media, and the SPR remained the same in all the samples. However, certain NPs, namely 1@AuNPs, 2@AuNPs, and 3@AuNPs, exhibited lower stability in cysteine. Additionally, the last one (3@AuNPs) was found to be influenced by glycine. After 24 h of incubation with BSA, most of the NPs exhibited an increase in their absorbance bands. This observed increment can be attributed to the direct interaction between the phenolic hydroxyl groups of the AuNP conjugates and the amino acids. Furthermore, BSA contains thiol groups that can interact with the metal surface, providing an additional factor contributing to the observed enhancement. AuNPs synthesized using procyanidin dimer showed the same effect [52].

Due to its diverse pharmacological effects, licorice has been used medicinally in South-East Asia/East Asia/the Middle East/Asia [53,54]. The plant has several physiologically

active compounds, with the following being the most abundant: triterpenoids, flavonoids, and polysaccharides [55]. These compounds are believed to be responsible for pharmacological effects, including antitumor, antiviral, anti-inflammatory, cardiovascular protection, antitussive, hepatoprotection, immunoregulatory, neuroprotective, and skin-protective effects [56–58]. It demonstrates notable effects, including its role as an antidepressant [51–54], neuroprotective agent [49,52,55,56], anticancer compounds [57,58], and anti-inflammatory active agent.

Liquiritin, a compound extracted from licorice, is known for its diverse range of pharmacological activities. It demonstrates antidepressant [59–62], neuroprotective [57,60,63,64], anticancer [65,66], and anti-inflammatory activities [2,55,61]. Additionally, isoliquiritin has been found to have antidepressant [62], antiangiogenic [67], neuroprotective [68], and wound healing [69] properties. Neoisoliquiritin has been identified for its antitumor effects [70,71], and isoliquiritin apioside has demonstrated antigenotoxic [71] and antiangiogenic [72] activities. Liquiritin apioside has proven effective in protecting against epithelial injury in chronic obstructive pulmonary disease [73], and has antitussive [74] properties. Lastly, glabridin has shown anti-inflammatory, anti-atherogenic, estrogenic-like effects and a high capacity to regulate energy metabolism [75].

Macrophages are among the first immune cells that pathogens encounter upon entering the body. As a result, the body experiences an inflammatory response, leading to the re-establishment of normal tissue structure and function [76]. Therefore, the RAW 264.7 cell line was selected to evaluate the bioactivity of the licorice extract, compounds, and nanoparticles, as the cell line has been used to predict the potential effect of natural products for their bioactivity on primary cells or in vivo [77].

This study, to our knowledge, was the first time the total extract, isolated compounds, and their respective green synthesized AuNPs, liquiritin (1), isoliquiritin (2), neoisoliquiritin (3), isoliquiritin apioside (4), liquiritin apioside (5), and glabridin (6) were all screened in one study to assess their potential effects on cell viability and the inflammatory biomarker, NO, using murine cell line RAW 264.7 macrophages.

The TE was not cytotoxic nor did it exhibit any effect on inflammation at all concentrations under both conditions (Figure 2). Comparably, under basal conditions, the AuNPs increased NO secretion from the cells at concentrations $\geq 50 \mu\text{g}/\text{mL}$ (Figure 2m). It is considered that AuNPs induces inflammation in RAW cells by mediating reactive oxygen species (ROS) and nuclear factor $\kappa\beta$ (NF- $\kappa\beta$) signaling pathways which lead to the production of inflammatory cytokines such as COX-2, IL-6, and TNF- α [78]. The induction of NO under basal conditions was also seen at 4@AuNP ($\geq 12.5 \mu\text{g}/\text{mL}$). Although the total extract was non-toxic and did not affect inflammation, the isolated compounds and their respective AuNPs showed various degrees of cytotoxicity and inflammatory responses. The nontoxic effects of the total extracts explain the wide range of activity, especially antiviral and anti-inflammatory, as mentioned above. From the chemical point of view, the presence of a plethora of pharmacologically active compounds in the extract makes it behave differently from the isolated pure compounds described in this study; other compounds such as triterpenoids and flavonoids may play a role in determining the ultimate biological activity.

The compounds liquiritin (1) and liquiritin apioside (5) decreased cell viability at concentrations $\geq 50 \mu\text{g}/\text{mL}$ in the absence of LPS (Figure 2a,i). A similar trend was seen when liquiritin (1) was exposed to human liver cells, HepG2, for 24 hrs. The authors demonstrated that HepG2 viability was decreased to below 40% at concentrations $\geq 120 \mu\text{M}$. Chen et al. [79] also reported a decrease in cell viability when PC12 cells in the presence of neuronal growth factor were exposed to liquiritin over 3- and 5-day periods at concentrations $\geq 50 \mu\text{g}/\text{mL}$ [63]. Liquiritin apioside (5) did not affect RAW cell proliferation under a simulated inflammatory response (Figure 2i). However, cell proliferation was hampered in the absence of LPS at concentrations $\geq 50 \mu\text{g}/\text{mL}$. Although not assessed in the study, it is proposed that liquiritin (1), and possibly liquiritin apioside (5), induces cell apoptosis by activating the caspases, setting off a cascade reaction that subsequently coor-

indicates cell death as seen in cell lines such as A549 and rheumatoid arthritis fibroblast-like synoviocytes [56,61,65,80].

When 1@AuNPs were exposed to the RAW cells, the level of cytotoxicity decreased, as it was exhibited only at 100 $\mu\text{g}/\text{mL}$ in the presence of LPS (Figure 2a), depicting the mitogenic effect of LPS. Studies by Weng et al. and Wang et al. established a liquiritin-loaded micelle and liquiritin-loaded precursor liposome, where the bioavailability was greater than liquiritin itself, in mice and rat models, respectively, which could explain the above phenomena, albeit in vitro [81,82]. Conversely, when 5@AuNPs were exposed to RAW cells, they exhibited more significant toxicity than 1@AuNPs as they were toxic at concentrations $\geq 3.125 \mu\text{g}/\text{mL}$ and 100 $\mu\text{g}/\text{mL}$ in the absence or presence of LPS. This could be due to the enhanced uptake of the particles into the cell. This observation may support the direct effect of AuNPs for enhancing the activity of natural compounds even if the compound is hydrophilic.

Isoliquiritin (2) alone reduced cell viability at 100 $\mu\text{g}/\text{mL}$ in the absence of LPS, with no effect on viability when stimulated with LPS (Figure 2c). Zhou and Ho found that isoliquiritin upregulated Bax and Bid proteins as well as increasing caspase activity in A549 lung fibroblasts [80]. This could be attributed to what was seen at 100 $\mu\text{g}/\text{mL}$. It was also found that exposure of isoliquiritin to B65 neuroblastomas reduced viability at 100 μM after 48 h [57], whereas two studies reported that RAW 264.7 cell viability was not affected when exposed to 0–1.6 μM or 0–200 μM isoliquiritin (2) for 24 h, contradicting the findings in this study [76,83]. This discrepancy in viability could be attributed to the differences in concentration ranges assessed in our study. Isoliquiritin (2) possesses a sugar moiety, thereby reducing its lipophilicity and compatibility with the RAW cellular membrane, as the affinity for the cell membrane plays a role in the uptake of lipophilic compounds by passive diffusion [76]. However, when isoliquiritin (2) was conjugated to the AuNPs, the level of cytotoxicity increased at concentrations $\geq 12.5 \mu\text{g}/\text{mL}$ and $\geq 50 \mu\text{g}/\text{mL}$ when unstimulated or stimulated by LPS, respectively (Figure 2c). The observed activity of the conjugated 2@AuNPs supports the role of AuNPs in increasing the activity of the capping agent, most probably through the formation of a proactive form at the surface of the magnetic nanoparticles (MNPs), thereby making it more compatible with the cell membrane and promoting the uptake of the NPs.

The chalcone glycoside, isoliquiritin apioside (4), did not impact cell viability in the absence of LPS. These results were corroborated by Kim and Ma, who found that up to 100 μM of isoliquiritin apioside (4) did not affect cell proliferation of human epithelial cells (HT1080) [72]. However, when in the presence of LPS, viability was reduced between 60 and 70% when exposed to 25 and 50 $\mu\text{g}/\text{mL}$ isoliquiritin apioside (Figure 2g). An extensive review by Dhaliwal et al. stipulated that chalcones such as isoliquiritin apioside (4) can cause loss of cell viability and mitochondrial membrane potential while inducing morphological changes consistent with apoptosis [84]. Further tests are needed to explain the reduced viability at the concentrations mentioned above. The non-toxic nature of isoliquiritin apioside (4) was further compounded when attached to the AuNPs, as proliferation was not impacted across all concentrations and under all conditions assessed.

The prenylated isoflavonoid glabridin (6) is a phytoestrogen and acts via estrogen receptors, which RAW 264.7 cells have been shown to express [75,85]. This would indicate the route via which the compound is taken into the cells and exerts its toxicity. This was seen at concentrations $> 25 \mu\text{g}/\text{mL}$ of glabridin (6) and glabridin conjugated to the AuNPs (Figure 2j). Cellular experiments have shown that glabridin induces cancer cell apoptosis by activating the mitochondrial apoptotic pathway and the caspase cascade [86]. However, evidence has been contradictory as glabridin promoted MC3T3-E1 cell proliferation and neuroprotection [87].

In brief, the RAW cells exposed to the purified components of licorice without LPS experienced different cytotoxic sensitivities: liquiritin (1) $>$ liquiritin apioside (5) $>$ glabridin (6) $>$ isoliquiritin (2). However, in the presence of LPS, the sensitivity of RAW cell viability differed from that of the unstimulated samples. These sensitivities were glabridin (6) $>$

isoliquiritin apioside (4) > liquiritin (1). The RAW cells were sensitive to three of the seven AuNPs in the absence of LPS: 5@AuNPs > 2@AuNPs > 6@AuNPs. In the presence of LPS, the cells were sensitive to 2@AuNPs > 6@AuNPs > 1@AuNPs > 5@AuNPs.

When the RAW cells were challenged with LPS and subsequently treated with the various compounds, the inflammatory marker NO was monitored at non-toxic concentrations. The reduction of NO by the compounds occurred at different concentrations: liquiritin (≥ 25 $\mu\text{g}/\text{mL}$) and glabridin (≥ 12.5 $\mu\text{g}/\text{mL}$) (Figure 2). Interestingly, the methanolic extract did not reduce inflammation in comparison to the isolated compounds. These results are in line with the reported anti-inflammatory properties of the compounds. Liquiritin was shown to reduce the phosphorylation of NF- κ B when THP-1 monocytic cells were stimulated with LPS. This subsequently reduced the monitored inflammatory markers IL-6, TNF-, and IL-1 [58]. Gao et al. reported that liquiritin inhibited protein and mRNA levels of the inflammatory cytokines IL-6 and IL-8 in IL-1 in stimulated SW982 human synovial cells [55]. They showed that liquiritin can suppress inflammation across cell types, and Wang et al. further compounded this as NF- κ B was reduced in HepG2 cells [79]. Chen et al. provided insight into the mechanism employed by liquiritin apioside in RAW 264.7 cells as they were shown to suppress the PI3K/Akt/NF- κ B pathways responsible for inflammation [70]. By inhibiting this pathway in macrophages, the expression of inducible nitric oxide synthase (iNOS) and NO production in LPS-induced RAW 264.7 cells was inhibited [86]. Subsequent studies have also reported the decrease of inflammation via inhibiting the NF- κ B pathway by the other compounds: isoliquiritin, isoliquiritin apioside, and glabridin [72,75,83,84]

The subsequent AuNPs conjugated to the various compounds also reduced inflammatory activity: 2@AuNPs (12.5 $\mu\text{g}/\text{mL}$) and 6@AuNPs (≥ 12.5 $\mu\text{g}/\text{mL}$) (Figure 2). The reduction in inflammation associated with the NPs is postulated to occur via the NF- κ B pathway, as previously mentioned in the discussion. This can be inferred through other limited studies monitoring the anti-inflammatory activity on RAW cells exposed to other green synthesized AuNPs. These studies noted that *Euphrasia officinalis*, *Suaeda japonica* and chitosan–ginsenoside compound K (CK) AuNPs reduced inflammatory activity by the following mechanisms: inhibiting the iNOS and COX-2 mRNA levels; decreasing the phosphorylation and degradation of inhibitor kappa beta; decreasing the nuclear translocation of NF- κ B 65 and p50, and inhibiting the JAK/STAT pathway [88,89]. In certain cases, the NPs reduced inflammation at lower concentrations, as in the case of 2@AuNPs. This could be due to the increased uptake of the AuNPs by the RAW cells. Further studies will be needed to explore and establish how the NPs are taken up and, if so, where they are located in the cell.

In synopsis, when challenged with LPS, the anti-inflammatory potential of the compounds ranged in the order liquiritin (1) \leq glabridin (6). The anti-inflammatory potential of the compounds conjugated to the AuNPs ranged in the order 6@AuNPs \leq 2@AuNPs in the presence of LPS.

There were limitations to this study as it was a pilot study. In future studies, we aim to monitor cellular uptake and the intracellular morphology of cells exposed to AuNPs. In addition, other inflammatory biomarkers and oxidative stress biomarkers will be assessed.

5. Conclusions

Phenolic compounds can form, stabilize, and activate AuNPs due to their flexibility in donating electrons and the formation of proactive forms at the surface of the AuNPs. The interaction at the surface of the nanoparticles caused a shift in activity for some of the AuNP conjugates from their intact capping agents, as shown by liquiritin in this study. In most cases, the individual compounds exhibited a more potent anti-inflammatory response than the total methanolic extract or their AuNP counterpart. Although certain compounds exhibited a greater anti-inflammatory response, they were also more cytotoxic than the extract and their relative AuNPs. As suggested by the results, the 2@AuNP conjugate exhibited the highest anti-inflammatory potency compared with the other samples, necessitating

further investigation to elucidate its potential as a candidate for inflammation treatment. Utilizing individual, well-characterized natural products with established pharmacological properties represents a significant alternative to employing entire extracts. This approach allows precise control over variable factors and facilitates the design and prediction of metallic nanoparticles.

Supplementary Materials: The following supporting information can be downloaded at <https://www.mdpi.com/article/10.3390/jfb15040095/s1>. Figure S1. LC-MS chromatogram of the total extract and the tentative identification of the major compounds [90–95]. Figure S2.1. ^1H and ^{13}C spectra of compound 1. Figure S2.2. ^1H and ^{13}C spectra of compound 2. Figure S2.3. ^1H and ^{13}C spectra of compound 3. Figure S2.4. ^1H and ^{13}C spectra of compound 4. Figure S2.5. ^1H and ^{13}C spectra of compound 5. Figure S2.6. ^1H and ^{13}C spectra of compound 6. Figure S3. Ultraviolet-visible spectra of the green synthesized AuNP conjugates and the intact extract/pure compounds. Figure S4. Zeta potential and relative size distribution of the synthesized NPs. Figure S5. HRTEM of the synthesized AuNPs. Figure S6. Stability of the AuNP conjugates in different biogenic media after 24 h. Figure S7. Stability of the AuNP conjugates for three months. Figure S8. XRD of the synthesized AuNPs. Figure S9. FTIR spectra of the synthesized AuNPs with their intact compounds. Figure S10. FTIR of total extract/pure compounds (black) and their corresponding AuNPs (red) in the 1700–930 cm^{-1} range. Table S1. The calculation using Scherrer equation.

Author Contributions: Conceptualization, A.A.H.; methodology, A.O.E.E., K.L.L. and O.M.D.; validation, A.A.H., K.L.L. and O.M.D.; formal analysis, K.L.L., O.M.D. and A.A.H.; investigation, K.L.L., A.O.E.E. and O.M.D.; resources, A.A.H., R.C.L. and E.J.P.; data curation, A.A.H., K.L.L. and O.M.D.; writing—original draft preparation, A.O.E.E., K.L.L. and O.M.D.; writing—review and editing, A.A.H., K.L.L. and E.J.P.; supervision, A.A.H. and R.C.L.; project administration, A.A.H.; funding acquisition, A.A.H., R.C.L. and E.J.P. All authors have read and agreed to the published version of the manuscript.

Funding: This research was funded by the National Research Foundation, South Africa, grant number [106055], and The APC was funded by the University of Western Cape, the University of Stellenbosch and the Cape Peninsula University of Technology.

Data Availability Statement: The 2D NMR spectra will be made available by the corresponding author on request.

Acknowledgments: Omdurman Islamic University (Sudan) for supporting AOEE and Cape Peninsula University of Technology for the NMR facility.

Conflicts of Interest: The authors declare no conflict of interest.

References

1. Satyanarayana, T.; Reddy, S. A review on chemical and physical synthesis methods of nanomaterials. *Int. J. Res. Appl. Sci. Eng. Technol.* **2018**, *6*, 2885–2889. [[CrossRef](#)]
2. Yu, J.-Y.; Ha, J.Y.; Kim, K.-M.; Jung, Y.-S.; Jung, J.-C.; Oh, S. Anti-inflammatory activities of licorice extract and its active compounds, glycyrrhizic acid, liquiritin and liquiritigenin, in BV2 cells and mice liver. *Molecules* **2015**, *20*, 13041–13054. [[CrossRef](#)] [[PubMed](#)]
3. Yaqoob, S.B.; Adnan, R.; Khan, R.M.R.; Rashid, M. Gold, silver, and palladium nanoparticles: a chemical tool for biomedical applications. *Front. Chem.* **2020**, *8*, 376. [[CrossRef](#)] [[PubMed](#)]
4. Hwang, S.J.; Jun, S.H.; Park, Y.; Cha, S.-H.; Yoon, M.; Cho, S.; Lee, H.-J.; Park, Y. Green synthesis of gold nanoparticles using chlorogenic acid and their enhanced performance for inflammation. *Nanomed. Nanotechnol. Biol. Med.* **2015**, *11*, 1677–1688. [[CrossRef](#)] [[PubMed](#)]
5. Muller, A.P.; Ferreira, G.K.; Pires, A.J.; Silveira, G.D.B.; Souza, D.L.D.; Brandolfi, J.D.A.; Souza, C.T.D.; Paula, M.M.; Silveira, P.C.L. Gold nanoparticles prevent cognitive deficits, oxidative stress and inflammation in a rat model of sporadic dementia of Alzheimer's type. *Mater. Sci. Eng. C* **2017**, *77*, 476–483. [[CrossRef](#)] [[PubMed](#)]
6. Filip, G.A.; Moldovan, B.; Baldea, I.; Olteanu, D.; Suharoschi, R.; Decea, N.; Cismaru, C.M.; Gal, E.; Cenariu, M.; Clichici, S.; et al. UV-light mediated green synthesis of silver and gold nanoparticles using Cornelian cherry fruit extract and their comparative effects in experimental inflammation. *J. Photochem. Photobiol. B Biol.* **2019**, *191*, 26–37. [[CrossRef](#)] [[PubMed](#)]
7. Liu, Y.; Kim, S.; Kim, Y.J.; Perumalsamy, H.; Lee, S.; Hwang, E.; Yi, T.-H. Green synthesis of gold nanoparticles using Euphrasia officinalis leaf extract to inhibit lipopolysaccharide-induced inflammation through NF- κ B and JAK/STAT pathways in RAW 264.7 macrophages. *Int. J. Nanomed.* **2019**, *14*, 2945–2959. [[CrossRef](#)] [[PubMed](#)]

8. Agarwal, H.; Nakara, A.; Shanmugam, V.K. Anti-inflammatory mechanism of various metal and metal oxide nanoparticles synthesized using plant extracts: A review. *Biomed. Pharmacother.* **2019**, *109*, 2561–2572. [[CrossRef](#)] [[PubMed](#)]
9. Alegria, E.C.B.A.; Ribeiro, A.P.C.; Mendes, M.; Ferraria, A.M.; Rego, A.M.B.D.; Pombeiro, A.J.L. Effect of phenolic compounds on the synthesis of gold nanoparticles and its catalytic activity in the reduction of nitro compounds. *Nanomaterials* **2018**, *8*, 320. [[CrossRef](#)]
10. Ho, B.N.; Pfeffer, C.M.; Singh, A.T. Update on nanotechnology-based drug delivery systems in cancer treatment. *Anticancer Res.* **2017**, *37*, 5975–5981.
11. Yi, D.K.; Nanda, S.S.; Kim, K.; Selvan, S.T. Recent progress in nanotechnology for stem cell differentiation, labeling, tracking and therapy. *J. Mater. Chem. B* **2017**, *5*, 9429–9451. [[CrossRef](#)] [[PubMed](#)]
12. Javed, R.; Sajjad, A.; Naz, S.; Sajjad, H.; Ao, Q. Significance of capping agents of colloidal nanoparticles from the perspective of drug and gene delivery, bioimaging, and bi-sensing: an insight. *Int. J. Mol. Sci.* **2022**, *23*, 10521. [[CrossRef](#)]
13. Nune, S.K.; Chanda, N.; Shukla, K.K.R.; Kulkarni, R.R.; Thilakavathi, S.; Mekapothula, S.; Kannan, R.; Katti, K.V. Green nanotechnology from tea: phytochemicals in tea as building blocks for production of biocompatible gold nanoparticles. *J. Mater. Chem.* **2009**, *19*, 2912–2920. [[CrossRef](#)] [[PubMed](#)]
14. Khoobchandani, M.; Khan, A.; Katti, K.K.; Amal, Y.V.C.; MohanDoss, D.K.D.; Nicholl, M.B.; Lugão, A.B.; Han, C.P.; Katti, K. Green nanotechnology of MGF-AuNPs for immunomodulatory intervention in prostate cancer therapy. *Sci. Rep.* **2021**, *11*, 16797. [[CrossRef](#)] [[PubMed](#)]
15. Bollella, P.; Schulz, C.; Favero, G.; Mazzei, F.; Ludwig, R.; Gorton, L.; Antiochia, R. Green synthesis and characterization of gold and silver nanoparticles and their application for development of a third generation lactose biosensor. *Electroanalysis* **2017**, *29*, 77–86. [[CrossRef](#)]
16. Biao, L.; Tan, S.; Meng, Q.; Gao, J.; Zhang, X.; Fu, Y. Green synthesis, characterization and application of proanthocyanidins-functionalized gold nanoparticles. *Nanomaterials* **2018**, *8*, 53. [[CrossRef](#)]
17. Elbagory, A.M.; Hussein, A.A.; Meyer, M. The in vitro immunomodulatory effects of gold nanoparticles synthesized from hypoxis hemerocallidea aqueous extract and hypoxoside on macrophage and natural killer cells. *Int. J. Nanomed.* **2019**, *19*, 9007–9018. [[CrossRef](#)] [[PubMed](#)]
18. Badeggi, U.M.; Omoruyi, S.I.; Ismail, E.; Africa, C.; Botha, S.; Hussein, A.A. Characterization and toxicity of hypoxoside capped silver nanoparticles. *Plants* **2022**, *11*, 1037. [[CrossRef](#)]
19. Pradhan, S.P.; Sahoo, S.; Behera, A.; Sahoo, R.; Sahu, P.K. Memory amelioration by hesperidin conjugated gold nanoparticles in diabetes induced cognitive impaired rats. *J. Drug Deliv. Sci. Technol.* **2022**, *69*, 103145. [[CrossRef](#)]
20. Sulaiman, G.; Waheeb, H.M.; Jabir, M.S.; Khazaal, S.H.; Dewir, Y.H.; Naidoo, Y. Hesperidin loaded on gold nanoparticles as a drug delivery system for a successful biocompatible, anti-cancer, anti-inflammatory and phagocytosis inducer model. *Sci. Rep.* **2020**, *10*, 9362. [[CrossRef](#)]
21. Alsamhary, K.; Al-Enazi, N.; Alshehr, W.A.; Ameen, F. Gold nanoparticles synthesised by flavonoid tricetin as a potential antibacterial nanomedicine to treat respiratory infections causing opportunistic bacterial pathogens. *Microb. Pathog.* **2020**, *139*, 103928. [[CrossRef](#)] [[PubMed](#)]
22. Pedroso-Santana, S.; Fleitas-Salazar, N. The use of capping agents in the stabilization and functionalization of metallic nanoparticles for biomedical applications. *Part. Part. Syst. Charact.* **2023**, *40*, 2200146. [[CrossRef](#)]
23. Leonard, K.; Ahmmad, B.; Okamura, H.; Kurawaki, J. In situ green synthesis of biocompatible ginseng capped gold nanoparticles with remarkable stability. *Colloids Surf. B Biointerfaces* **2011**, *82*, 391–396. [[CrossRef](#)] [[PubMed](#)]
24. Minatel, I.O.; Borges, C.V.; Ferreira, M.I.; Gomez, H.A.G.; Chen, C.-Y.O.; Lima, G.P.P. Phenolic compounds: Functional properties, impact of processing and bioavailability. In *Phenolic Compounds—Biological Activity*; Soto-Hernandez, M., Palma-Tenango, M., del Rosario Garcia-Mateos, M., Eds.; InTech: London, UK, 2017; pp. 1–238.
25. Tungmunthum, D.; Thongboonyou, A.; Pholboon, A.; Yangsabai, A. Flavonoids and other phenolic compounds from medicinal plants for pharmaceutical and medical aspects: An overview. *Medicines* **2018**, *5*, 93. [[CrossRef](#)] [[PubMed](#)]
26. Mamedov, N.A.; Egamberdieva, D. Phytochemical constituents and pharmacological effects of licorice: A review. *Plant Hum. Health* **2019**, *3*, 1–21.
27. Hasan, M.K.; Ara, I.; Mondal, M.S.A.; Kabi, Y. Phytochemistry, pharmacological activity, and potential health benefits of *Glycyrrhiza glabra*. *Heliyon* **2021**, *7*, e07240. [[CrossRef](#)] [[PubMed](#)]
28. Ullah, A.; Munir, S.; Badshah, S.L.; Khan, N.; Ghani, L.; Poulson, B.G.; Emwas, A.-H.; Jaremko, M. Important flavonoids and their role as a therapeutic agent. *Molecules* **2020**, *25*, 5243. [[CrossRef](#)] [[PubMed](#)]
29. Nirmala, P.; Selvaraj, T. Anti-inflammatory and anti-bacterial activities of *Glycyrrhiza glabra* L. *J. Agric. Technol.* **2011**, *7*, 815–823.
30. Leite, C.D.S.; Bonafé, G.A.; Santos, J.C.; Martinez, C.A.R.; Ortega, M.M.; Ribeiro, M.L. The anti-inflammatory properties of licorice (*glycyrrhiza glabra*)-derived compounds in intestinal disorders. *Int. J. Mol. Sci.* **2022**, *23*, 4121. [[CrossRef](#)]
31. Elbagory, A.M.; Cupido, C.N.; Meyer, M.; Hussein, A.A. Large scale screening of southern african plant extracts for the green synthesis of gold nanoparticles using microtitre-plate method. *Molecules* **2016**, *21*, 1498. [[CrossRef](#)]
32. Sorci, G.; Faivre, B. Inflammation and oxidative stress in vertebrate host–parasite systems. *Philos. Trans. R. Soc. B Biol. Sci.* **2009**, *364*, 71–83. [[CrossRef](#)] [[PubMed](#)]
33. Libert, S.; Chao, Y.; Chu, X.; Pletcher, S.D. Trade-offs between longevity and pathogen resistance in *Drosophila melanogaster* mediated by NFκB signalling. *Aging Cell* **2006**, *5*, 533–543. [[CrossRef](#)]

34. Brenner, D.R.; Scherer, D.; Muir, K.; Schildkraut, J.; Boffetta, P.; Spitz, M.R.; Marchand, L.L.; Chan, A.T.; Goode, E.L.; Ulrich, C.M.; et al. A review of the application of inflammatory biomarkers in epidemiologic cancer research. *Cancer Epidemiol. Biomark. Prev.* **2014**, *23*, 1729–1751. [[CrossRef](#)]
35. Lategan, K.; Alghadi, H.; Bayati, M.; Cortalezzi, M.F.D.; Pool, E. Effects of graphene oxide nanoparticles on the immune system biomarkers produced by raw 264.7 and human whole blood cell cultures. *Nanomaterials* **2018**, *8*, 125. [[CrossRef](#)] [[PubMed](#)]
36. Gasparrini, M.; Forbes-Hernandez, T.Y.; Giampieri, F.; Afrin, S.; Alvarez-Suarez, J.M.; Mazzoni, L.; Mezzetti, B.; Quiles, J.L.; Battino, M. Anti-inflammatory effect of strawberry extract against LPS-induced stress in RAW 264.7 macrophages. *Food Chem. Toxicol.* **2017**, *102*, 1–10. [[CrossRef](#)] [[PubMed](#)]
37. Yu, Y.; Correll, P.H.; Heuvel, J.P.V. Conjugated linoleic acid decreases production of pro-inflammatory products in macrophages: Evidence for a PPAR gamma-dependent mechanism. *Biochim. Biophys. Acta* **2002**, *1581*, 89–99. [[CrossRef](#)]
38. Hwang, S.J.; Kim, Y.-W.; Park, Y.; Lee, H.-J.; Kim, K.-W. Anti-inflammatory effects of chlorogenic acid in lipopolysaccharide-stimulated RAW 264.7 cells. *Inflamm. Res.* **2014**, *63*, 81–90. [[CrossRef](#)] [[PubMed](#)]
39. Chiou, W.-F.; Chen, C.-F.; Lin, J.-J. Mechanisms of suppression of inducible nitric oxide synthase (iNOS) expression in RAW 264.7 cells by andrographolide. *Br. J. Pharmacol.* **2000**, *129*, 1553–1560. [[CrossRef](#)]
40. Sharma, J.N.; Al-Omran, A.; Parvathy, S.S. Review role of nitric oxide in inflammatory diseases. *Inflammopharmacology* **2007**, *15*, 252–259. [[CrossRef](#)]
41. Aktan, F. iNOS-mediated nitric oxide production and its regulation and its regulation. *Life Sci.* **2004**, *75*, 639–653. [[CrossRef](#)]
42. Dubey, S.P.; Lahtinen, M.; Sillanpää, M. Green synthesis and characterizations of silver and gold nanoparticles using leaf extract of *Rosa rugosa*. *Colloids Surf. A Physicochem. Eng. Asp.* **2010**, *364*, 34–41. [[CrossRef](#)]
43. Aryal, S.; Remant, B.K.C.; Dharmaraj, N.; Bhattarai, N.; Kim, C.H.; Kim, H.Y. Spectroscopic identification of S-Au interaction in cysteine capped gold nanoparticles. *Spectrochim. Acta Part A Mol. Biomol. Spectrosc.* **2006**, *63*, 160–163. [[CrossRef](#)] [[PubMed](#)]
44. Kaur, P.; Kaur, S.; Kumar, N.; Singh, B.; Kumar, S. Evaluation of antigenotoxic activity of isoliquiritin apioside from *Glycyrrhiza glabra* L. *Toxicol. Vitro.* **2009**, *23*, 680–686. [[CrossRef](#)] [[PubMed](#)]
45. Guo, Z.; Niu, X.; Xiao, T.; Lu, J.; Li, W.; Zhao, Y. Chemical profile and inhibition of α -glycosidase and protein tyrosine phosphatase 1B (PTP1B) activities by flavonoids from licorice (*Glycyrrhiza uralensis* Fisch.). *J. Funct. Foods* **2015**, *14*, 324–336. [[CrossRef](#)]
46. Ji, S.; Li, Z.; Song, W.; Wang, Y.; Liang, W.; Li, K.; Tang, S.; Wang, Q.; Qiao, X.; Zhou, D.; et al. Bioactive constituents of glycyrrhiza uralensis (licorice): Discovery of the effective components of a traditional herbal medicine. *J. Nat. Prod.* **2016**, *79*, 281–292. [[CrossRef](#)] [[PubMed](#)]
47. Kletsov, A.; Dahnovsky, Y.; Ortiz, J.V. Surface Green's function calculations: A nonrecursive scheme with an infinite number of principal layers. *J. Chem. Phys.* **2007**, *126*, 134105. [[CrossRef](#)]
48. Binzel, D.W.; Li, X.; Burns, N.; Khan, E.; Lee, W.-J.; Chen, L.-C.; Ellipilli, S.; Miles, W.; Ho, Y.S.; Guo, P. Thermostability, tunability, and tenacity of RNA as rubbery anionic polymeric materials in nanotechnology and nanomedicine specific cancer targeting with undetectable toxicity. *Chem. Rev.* **2021**, *121*, 7398–7467. [[CrossRef](#)]
49. Heo, D.N.; Yang, D.H.; Moon, H.-J.; Lee, J.B.; Bae, M.S.; Lee, S.C.; Lee, W.J.; Sun, I.-C.; Kwon, I.K. Gold nanoparticles surface-functionalized with paclitaxel drug and biotin receptor as theranostic agents for cancer therapy. *Biomaterials* **2012**, *33*, 856–866. [[CrossRef](#)] [[PubMed](#)]
50. Al-Yasiri, A.Y.; Khoobchandani, M.; Cutler, C.S.; Watkinson, L.; Carmack, T.; Smith, C.J.; Kuchuk, M.; Loyalka, S.K.; Lugão, A.B.; Katti, K.V. Mangiferin functionalized radioactive gold nanoparticles (MGF-¹⁹⁸AuNPs) in prostate tumour therapy: Green nanotechnology for production, in vivo tumour retention and evaluation of therapeutic efficacy. *Dalton Trans.* **2017**, *46*, 14561–14571. [[CrossRef](#)]
51. Wongsu, P.; Phatikulrungsun, P.; Prathumthong, S. FT-IR characteristics, phenolic profiles and inhibitory potential against digestive enzymes of 25 herbal infusions. *Sci. Rep.* **2022**, *12*, 6631. [[CrossRef](#)]
52. Badeggi, U.M.; Ismail, E.; Adeloye, A.O.; Botha, S.; Badmus, J.A.; Marnewick, J.L.; Cupido, C.N.; Hussein, A.A. Green synthesis of gold nanoparticles capped with procyanidins from leucosidea sericea as potential antidiabetic and antioxidant agents. *Biomolecules* **2020**, *10*, 452. [[CrossRef](#)]
53. Asano, T.; Ishihara, K.; Morota, T.; Takeda, S.; Aburada, M. Permeability of the flavonoids liquiritigenin and its glycosides in licorice roots and davidigenin, a hydrogenated metabolite of liquiritigenin, using human intestinal cell line Caco-2. *J. Ethnopharmacol.* **2003**, *89*, 285–289. [[CrossRef](#)] [[PubMed](#)]
54. Kojoma, M.; Hayashi, S.; Shibata, T.; Yamamoto, Y.; Sekizaki, H. Variation of glycyrrhizin and liquiritin contents within a population of 5-year-old licorice (*Glycyrrhiza uralensis*) plants cultivated under the same conditions. *Biol. Pharm. Bull.* **2011**, *34*, 1334–1337. [[CrossRef](#)]
55. Gao, Y.-X.; Cheng, B.-F.; Lian, J.-J.; Guo, D.-D.; Qin, J.-W.; Zhang, Y.-B.; Yang, H.-J.; Wang, M.; Wang, L.; Feng, Z.-W. Liquiritin, a flavone compound from licorice, inhibits IL-1 β -induced inflammatory responses in SW982 human synovial cells. *J. Funct. Foods* **2017**, *33*, 142–148. [[CrossRef](#)]
56. Qin, J.; Chen, J.; Peng, F.; Sun, C.; Lei, Y.; Chen, G.; Li, G.; Yin, Y.; Wu, Z.L.L.; Li, J.; et al. Pharmacological activities and pharmacokinetics of liquiritin: A review. *J. Ethnopharmacol.* **2022**, *293*, 115257. [[CrossRef](#)]
57. Nakatani, Y.; Kobe, A.; Kuriya, M.; Hiroki, Y.; Yahagi, T.; Sakakibara, I.; Matsuzaki, K.; Amano, T. Neuroprotective effect of liquiritin as an antioxidant via an increase in glucose-6-phosphate dehydrogenase expression on B65 neuroblastoma cells. *Eur. J. Pharmacol.* **2017**, *815*, 281–290. [[CrossRef](#)]

58. Liual, Z.; Wang, P.; Lu, S.; Guo, R.; Gao, W.; Tong, H.; Yin, Y.; Han, X.; Liu, T.; Chen, X.; et al. Liquiritin, a novel inhibitor of TRPV1 and TRPA1, protects against LPS-induced acute lung injury. *Cell Calcium* **2020**, *88*, 102198.
59. Zhao, Z.; Wang, W.; Guo, H.; Zhou, D. Antidepressant-like effect of liquiritin from *Glycyrrhiza uralensis* in chronic variable stress induced depression model rats. *Behav. Brain Res.* **2008**, *194*, 108–113. [[CrossRef](#)] [[PubMed](#)]
60. Sun, Y.-X.; Tang, Y.; Wu, A.-L.; Liu, T.; Dai, X.-L.; Zheng, Q.-S.; Wang, Z.-B. Neuroprotective effect of liquiritin against focal cerebral ischemia/reperfusion in mice via its antioxidant and antiapoptosis properties. *J. Asian Nat. Prod. Res.* **2010**, *12*, 1051–1060. [[CrossRef](#)]
61. Zhai, K.-F.; Duan, H.; Cui, C.-Y.; Cao, Y.-Y.; Si, J.-L.; Yang, H.-J.; Wang, Y.-C.; Cao, W.-G.; Gao, G.-Z.; Wei, Z.-J. Liquiritin from *glycyrrhiza uralensis* attenuating rheumatoid arthritis via reducing inflammation, suppressing angiogenesis, and inhibiting MAPK signaling pathway. *J. Agric. Food Chem.* **2019**, *67*, 2856–2864. [[CrossRef](#)]
62. Wang, W.; Hu, X.; Zhao, Z.; Liu, P.; Hu, Y.; Zhou, J.; Zhou, D.; Wang, Z.; Guo, H. Antidepressant-like effects of liquiritin and isoliquiritin from *Glycyrrhiza uralensis* in the forced swimming test and tail suspension test in mice. *Prog. Neuro-Psychopharmacol. Biol. Psychiatry* **2008**, *32*, 1179–1184. [[CrossRef](#)] [[PubMed](#)]
63. Chen, Z.-A.; Wang, J.-L.; Liu, R.-T.; Ren, J.-P.; Wen, L.-Q.; Chen, X.-J.; Bian, G.-X. Liquiritin potentiate neurite outgrowth induced by nerve growth factor in PC12 cells. *Cytotechnology* **2009**, *60*, 125–132. [[CrossRef](#)] [[PubMed](#)]
64. Yang, Y.; Bian, G.-X.; Lu, Q.-J. Neuroprotection and neurotrophism effects of liquiritin on primary cultured hippocampal cells. *China J. Chin. Mater. Medica* **2008**, *33*, 931–935.
65. Wei, F.; Jiang, X.; Gao, H.-Y.; Gao, S.-H. Liquiritin induces apoptosis and autophagy in cisplatin (DDP)-resistant gastric cancer cells in vitro and xenograft nude mice in vivo. *Int. J. Oncol.* **2017**, *51*, 1383–1394. [[CrossRef](#)] [[PubMed](#)]
66. He, S.-H.; Liu, H.-G.; Zhou, Y.-F.; Yue, Q.-F. Liquiritin (LT) exhibits suppressive effects against the growth of human cervical cancer cells through activating Caspase-3 in vitro and xenograft mice in vivo. *Biomed. Pharmacother.* **2017**, *92*, 215–228. [[CrossRef](#)] [[PubMed](#)]
67. Kobayashi, S.; Miyamoto, T.; Kimura, I.; Kimura, M. Inhibitory effect of isoliquiritin, a compound in licorice root, on angiogenesis in vivo and tube formation in vitro. *Biol. Pharm. Bull.* **1995**, *18*, 1382–1386. [[CrossRef](#)] [[PubMed](#)]
68. Zhou, Y.-Z.; Li, X.; Gong, W.-X.; Tian, J.-S.; Gao, X.-X.; Gao, L.; Zhang, X.; Du, G.-H.; Qin, X.-M. Protective effect of isoliquiritin against corticosterone-induced neurotoxicity in PC12 cells. *Food Funct.* **2017**, *8*, 1235–1244. [[CrossRef](#)]
69. Liu, Y.-Y.; Wu, J.-Q.; Fan, R.-Y.; He, Z.-H.; Li, C.-Y.; He, M.-F. Isoliquiritin promote angiogenesis by recruiting macrophages to improve the healing of zebrafish wounds. *Fish. Shellfish Immunol.* **2020**, *100*, 238–245. [[CrossRef](#)]
70. Chen, C.; Shao, R.; Li, B.; Zhai, Y.; Wang, T.; Li, X.; Miao, L.; Huang, J.; Liu, R.; Liu, E.; et al. Neoisoliquiritin exerts tumor suppressive effects on prostate cancer by repressing androgen receptor activity. *Phytomedicine* **2021**, *85*, 153514. [[CrossRef](#)]
71. Tang, H.; Peng, F.; Huang, X.; Xie, X.; Chen, B.; Shen, J.; Gao, F.; You, J.; Xie, X.; Chen, J. Neoisoliquiritigenin inhibits tumor progression by targeting GRP78- β -catenin signaling in breast cancer. *Curr. Cancer Drug Targets* **2018**, *18*, 390–399. [[CrossRef](#)]
72. Kim, A.; Ma, J.Y. Isoliquiritin apioside suppresses in vitro invasiveness and angiogenesis of cancer cells and endothelial cells. *Front. Pharmacol.* **2018**, *9*, 1455. [[CrossRef](#)]
73. Guan, Y.; Li, F.-F.; Hong, L.; Yan, X.-F.; Tan, G.-L.; He, J.-S.; Dong, X.-W.; Bao, M.-J.; Xie, Q.-M. Protective effects of liquiritin apioside on cigarette smoke-induced lung epithelial cell injury. *Fundam. Clin. Pharmacol.* **2012**, *26*, 473–483. [[CrossRef](#)] [[PubMed](#)]
74. Kuang, Y.; Li, B.; Fan, J.; Qiao, X.; Ye, M. Antitussive and expectorant activities of licorice and its major compounds. *Bioorg. Med. Chem.* **2018**, *16*, 278–284. [[CrossRef](#)]
75. Simmler, C.; Pauli, G.F.; Che, S.-N. Phytochemistry and biological properties of glabridin. *Fitoterapia* **2013**, *90*, 160–184. [[CrossRef](#)]
76. Kim, J.-Y.; Park, S.J.; Yun, K.-J.; Cho, Y.-W.; Park, H.-J.; Lee, K.-T. Isoliquiritigenin isolated from the roots of *Glycyrrhiza uralensis* inhibits LPS-induced iNOS and COX-2 expression via the attenuation of NF- κ B in RAW 264.7 macrophages. *Eur. J. Pharmacol.* **2008**, *584*, 175–184. [[CrossRef](#)] [[PubMed](#)]
77. Merly, L.; Smith, S.L. Murine RAW 264.7 cell line as an immune target: Are we missing something? *Immunopharmacol. Immunotoxicol.* **2017**, *39*, 55–58. [[CrossRef](#)] [[PubMed](#)]
78. Nishanth, R.P.; Prasad, T.; Jyotsna, R.G.; Reddy, P.K.; Reddanna, P. Inflammatory responses of RAW 264.7 macrophages upon exposure to nanoparticles: Role of ROS-NF κ B signaling pathway. *Nanotoxicology* **2011**, *5*, 502–516. [[CrossRef](#)]
79. Wang, J.-R.; Li, T.-Z.; Wang, C.; Li, S.-M.; Luo, Y.-H.; Piao, X.-J.; Feng, Y.-C.; Zhang, Y.; Xu, W.-T.; Zhang, Y.; et al. Liquiritin inhibits proliferation and induces apoptosis in HepG2 hepatocellular carcinoma cells via the ROS-mediated MAPK/AKT/NF- κ B signaling pathway. *Naunyn-Schmiedeberg's Arch. Pharmacol.* **2020**, *393*, 1987–1999. [[CrossRef](#)]
80. Zhou, Y.; Ho, W.S. Combination of liquiritin, isoliquiritin and isoliquirigenin induce apoptotic cell death through upregulating p53 and p21 in the A549 non-small cell lung cancer cells. *Oncol. Rep.* **2014**, *31*, 298–304. [[CrossRef](#)]
81. Weng, W.; Wang, Q.; Wei, C.; Adu-Frimong, M.; Torenizayov, E.; Ji, H.; Yu, J.; Xu, X. Mixed micelles for enhanced oral bioavailability and hypolipidemic effect of liquiritin: Preparation, in vitro and in vivo evaluation. *Drug Dev. Ind. Pharm.* **2021**, *47*, 308–318. [[CrossRef](#)]
82. Wang, Q.; Wei, C.; Weng, W.; Bao, R.; Adu-Frimong, M.; Torenizayov, E.; Ji, H.; Xu, X.-M.; Yua, J.N. Enhancement of oral bioavailability and hypoglycemic activity of liquiritin-loaded precursor liposome. *Int. J. Pharm.* **2021**, *592*, 120036. [[CrossRef](#)] [[PubMed](#)]

83. Wang, R.; Zhang, C.Y.; Bai, L.P.; Pan, H.D.; Shu, L.M.; Kong, A.-N.T.; Leung, E.L.-H.; Liu, L.; Li, T. Flavonoids derived from liquorice suppress murine macrophage activation by up-regulating heme oxygenase-1 independent of Nrf2 activation. *Int. Immunopharmacol.* **2015**, *28*, 917–924. [[CrossRef](#)] [[PubMed](#)]
84. Dhaliwal, J.S.; Moshawih, S.; Goh, K.W.; Loy, M.J.; Hossain, M.S.; Hermansyah, A.; Kotra, V.; Kifli, N.; Goh, H.P.; Dhaliwal, S.K.S.; et al. Pharmacotherapeutics applications and chemistry of chalcone derivatives. *Molecules* **2022**, *27*, 7062. [[CrossRef](#)] [[PubMed](#)]
85. Galal, N.; El-Beialy, W.R.; Deyama, Y.; Yoshimura, Y.; Suzuki, K.; Totsuka, Y. Novel effect of estrogen on RANK and c-fms expression in RAW 264.7 cells. *Int. J. Mol. Med.* **2007**, *20*, 97–101. [[CrossRef](#)] [[PubMed](#)]
86. Lia, C.-X.; Lia, T.-H.; Zhu, M.; Lai, J.; Wu, Z.-P. Pharmacological properties of glabridin (a flavonoid extracted from licorice): A comprehensive review. *J. Funct. Foods* **2021**, *85*, 104638. [[CrossRef](#)]
87. Choi, E.-M. The licorice root derived isoflavan glabridin increases the function of osteoblastic MC3T3-E1 cells. *Biochem. Pharmacol.* **2005**, *70*, 363–368. [[CrossRef](#)]
88. Kwak, G.Y.; Han, Y.; Baik, S.; Kong, B.M.; Yang, D.C.; Kang, S.C.; Sukweenadhi, J. Gold nanoparticles green-synthesized by the Suaeda japonica leaf extract and screening of anti-inflammatory activities on RAW 267.4 Macrophages. *Coatings* **2022**, *12*, 460. [[CrossRef](#)]
89. Mi, X.J.; Choi, H.S.; Park, H.R.; Kim, Y.J. Structural characterization and anti-inflammatory properties of green synthesized chitosan/compound K gold nanoparticles. *Int. J. Biol. Macromol.* **2022**, *213*, 247–258. [[CrossRef](#)] [[PubMed](#)]
90. Farag, M.A.; Porzel, A.; Wessjohann, L.A. Comparative metabolite profiling and fingerprinting of medicinal licorice roots using a multiplex approach of GC–MS, LC–MS and 1D NMR techniques. *Phytochemistry* **2012**, *76*, 60–72. [[CrossRef](#)]
91. Qiao, X.; Ji, S.; Yu, S.W.; Lin, X.H.; Jin, H.W.; Duan, Y.K.; Zhang, L.-R.; Guo, D.-A.; Min, Y. Identification of key licorice constituents which interact with cytochrome P450: Evaluation by LC/MS/MS cocktail assay and metabolic profiling. *AAPS J.* **2014**, *16*, 101–113. [[CrossRef](#)]
92. Zhang, M.; Deng, Y.; Wang, C.; Cai, H.L.; Wen, J.; Fang, P.F.; Zhang, B.-K.; Li, H.-D.; Yan, M. An LC–MS/MS method for determination of bioactive components of liquorice and Semen Strychni in rat plasma: Application to a pharmacokinetics study. *Drug Test. Anal.* **2018**, *10*, 262–271. [[CrossRef](#)] [[PubMed](#)]
93. Montoro, P.; Maldini, M.; Russo, M.; Postorino, S.; Piacente, S.; Pizza, C. Metabolic profiling of roots of liquorice (*Glycyrrhiza glabra*) from different geographical areas by ESI/MS/MS and determination of major metabolites by LC-ESI/MS and LC-ESI/MS/MS. *J. Pharm. Biomed. Anal.* **2011**, *54*, 535–544. [[CrossRef](#)] [[PubMed](#)]
94. Suzuki, T.; Tsukahara, M.; Akasaka, Y.; Inoue, H. A highly sensitive LC–MS/MS method for simultaneous determination of glycyrrhizin and its active metabolite glycyrrhetic acid: Application to a human pharmacokinetic study after oral administration. *Biomed. Chromatogr.* **2017**, *31*, e4032. [[CrossRef](#)] [[PubMed](#)]
95. Zhang, Q.; Ye, M. Chemical analysis of the Chinese herbal medicine Gan-Cao (licorice). *J. Chromatogr. A* **2009**, *1216*, 1954–1969. [[CrossRef](#)] [[PubMed](#)]

Disclaimer/Publisher’s Note: The statements, opinions and data contained in all publications are solely those of the individual author(s) and contributor(s) and not of MDPI and/or the editor(s). MDPI and/or the editor(s) disclaim responsibility for any injury to people or property resulting from any ideas, methods, instructions or products referred to in the content.